DISCLAIMER:

This document does not meet the
current format guidelines of
the Graduate School at
The University of Texas at Austin.

It has been published for
informational use only.

The Report Committee for Jairus Daniel Schwartz
Certifies that this is the approved version of the following report:

Model Comparison of Prototype Diesel Rotating Liner Engine And Baseline Diesel Engine

APPROVED BY
SUPERVISING COMMITTEE:

Supervisor:

Ronald Douglas Matthews

Matthew John Hall

Model Comparison of Prototype Diesel Rotating Liner Engine and Baseline Diesel Engine

by

Jairus Daniel Schwartz, BSME; MSE

Report

Presented to the Faculty of the Graduate School of

The University of Texas at Austin

in Partial Fulfillment

of the Requirements

for the Degree of

Master of Science in Engineering

The University of Texas at Austin

December, 2016

Dedication

To my parents, Andrew and Nicole, and brother Arik, who have always encouraged me to do my best and have given their unwavering support to me throughout my entire life.

To my close friends, Hobbs, Elyse, and D.R.

You all have made this report possible.

Acknowledgements

I would like to thank the many faculty members who have imparted valuable knowledge and skills to me in order to become a successful graduate student. I would like to thank Dr. Marcus Ashford who encouraged me to apply for graduate school at UT and fostered my engineering interests as an undergraduate. I would most importantly like to thank my supervisors, Dr. Matthews and Dr. Hall, who I have learned so much from and have helped guide me through my years as a graduate student. I would also like to thank Dr. Dardalis, the inventor of the Rotating Liner Engine, who allowed me to be a part of his innovative project.

Abstract

Modeling Comparison of Prototype Diesel Rotating Liner Engine and Baseline Diesel Engine

Jairus Daniel Schwartz, MSE

The University of Texas at Austin, 2016

Supervisor: Ronald Douglas Matthews

Frictional losses in combustion engines have been the subject of many automotive engineers' research. Understanding the fundamentals behind each frictional loss helps pave the way to finding a solution in reducing the overall frictional power losses and increasing efficiency. The reciprocating piston assembly has been proven to account for over 60% of all frictional power losses within a combustion engine. A major factor contributing to this is when the piston motion is temporarily static at top dead center (TDC) and bottom dead center (BDC). This causes the frictional forces between the cylinder wall and the piston rings to dramatically increase during these time periods.

A solution to this would be to rotate the cylinder wall in order to keep the frictional forces in the hydrodynamic regime throughout the entire cycle of the combustion engine process. The prototype diesel rotating liner engine (RLE) is designed to prove this concept. The prototype diesel RLE is a Cummins 4BT engine that has been converted to a single cylinder engine and uses a crank pulley and gear system to rotate the cylinder wall.

The purpose of this report is to provide information about the history of this research, a piston assembly friction model comparison between baseline engine and RLE, and a commercial application analysis. The results provide evidence of improved motoring operations and that a successfully operating prototype would be highly valued in the heavy-duty diesel industry.

Table of Contents

List of Tables x

List of Figures xi

CHAPTER 1: INTRODUCTION 1

1.A. Overview 1

1.B. Back Ground 2

1.B.1. The Spark Ignition Engine 2

1.B.2. The Compression Ignition Engine 5

1.B.3. Historical Use of Rotating Liners 6

1.C. Previous Research 9

1.C.1. Frictional Losses Within Piston Engines 9

1.C.2. Reducing Frictional Losses by Decreasing Oil Viscosity 14

1.D. The Rotating Liner Engine 16

CHAPTER 2: MODEL AND MODEL VERIFICATION OF ENGINE FRICTION AND FMEP 20

2.A. Overview 20

2.B. Models 21

2.B.1. The First Friction Models Developed by Bishop 21

2.B.2. Patton, Nitschke, and Heywood Models 23

2.B.3. Shayler, Leong, and Murphy Modifications to the Patton, Nitschke, and Heywood Models 27

2.B.4. Stanley, Taraza, Henein and Bryzik Simplified Piston Assembly Friction Model 29

CHAPTER 3: FRICTION TORQUE AND FMEP ESTIMATION 39

3.A. Rotating Liner Torque Estimation 40

3.A.1. Piston Ring Assembly Friction Contribution 40

3.A.2. Piston Skirt Friction Contribution....44
3.A.3. Liner Journal Bearing and Face Seal Contribution....46
3.A.4. Total Piston Assembly Friction Forces and Liner Torque....48
3.B. FMEP Estimation....52
3.B.1. Model Comparison....52
3.B.2. Estimated Cummins 4BT Baseline and RLE fmep....54
CHAPTER 4: COMMERCIAL APPLICATION....56
4.A. Potential Commercial Markets....56
4.A.1. Heavy Duty Diesel Engine Manufacturers....56
4.A.2. Global Ship and Boat Building....57
4.B. Market Interest....59
4.C. Competing Technologies....60
4.C.1. Lowering Oil Viscosity....60
4.C.2. Thermally Sprayed Protective Cylinder Coatings....61
4.D. Barriers to Market Entry....61
CHAPTER 5: CONCLUSIONS AND RECOMMENDATIONS....63
APPENDIX A: FUTURE CUMMINS 4BT PROTOTYPE RLE EXPERIMENTAL SETUP66
A.A. Future Experimentation....66
A.A.1. Heavy Duty Diesel RLE Prototype....66
A.A.2. Instrumentation....69
REFERENCES....72

List of Tables

Table 1.1. Baseline SI Engine Specifications. 17

Table 3.1. Cummins 4BT engine parameters.....39

Table 3.2. Piston skirt dimensions and parameters. 45

Table 3.3. Rotating liner journal bearing parameters. 47

Table A.1. Cummins 4BT engine parameters. 66

Table A.2. Torque sensor specifications. 71

Table A.3. List of NI modules used in Compact DAQ. 71

List of Figures

Figure 1.1. P-V Diagram of an ideal SI engine.....2

Figure 1.2. P-V Diagram of CI engine.....5

Figure 1.3. Sleeve valve engine design (Adams, 2010).....7

Figure 1.4. Bristol Hercules sleeve valve engine, http://www.sywellaerodrome.co.uk 2016.....8

Figure 1.5. Distribution of thermal energy released by gasoline combustion for a homogeneous charge SI engine for one load condition, neglecting parasitic losses (Burke, Neglar, Campbell, and Lundstrom, 1967). .10

Figure 1.6. Early friction experimental results (Cleveland and Bishop, 1960). 11

Figure 1.7. Forces acting on the top piston ring (Tamminen, Sandstrom, and Nurmi, 2005). 12

Figure 1.8. Stribeck diagram showing the regimes of friction for engine lubrication (Kim, Dardalis, Matthews, and Kiehne, 2005). 13

Figure 1.9. Effects of lowering oil viscosity (Cleveland and Bishop, 1960).....15

Figure 1.10. Alpha prototype RLE. 17

Figure 1.11. Baseline and RLE hot motoring friction torque measurements (Kim, Dardalis, Matthews, and Kiehne, 2005).....18

Figure 1.12. Tear down results of the baseline (left) and RLE (right) (Kim, Dardalis, Matthews, Kiehne, 2005).....19

Figure 2.1. Experimental results compared to model predictions for reciprocating piston friction (Sandoval amd Heywood, 2003).....27

Figure 2.2. Simplified Stribeck diagram.....30

Figure 2.3. Top ring (top left), second ring (bottom left), and oil ring (middle right) curvature profiles (Taraza, Henein, and Bryzik 2000). 32

Figure 2.4. Stribeck coefficients (Stanley, et al. 1999).....33
Figure 2.5. Fcp as a function of Scp (Stanley, et al. 1999).....35
Figure 2.6. Piston ring assembly friction model (red) vs. experiment (blue); 500 RPM, motored, no head (Stanley, et al. 1999). 36
Figure 2.7. Pisont ring assembly friction force (fired, no load) model (red) vs. experiment (blue), 850 RPM (Stanley, et al. 1999). 37
Figure 2.8. Skirt friction model (red) vs experiment (blue); 500 RPM, motored, no head (Stanley, et al. 1999).....37
Figure 3.1. Pressure trace of a heavy-duty diesel engine at 1000 rpm with no load.41
Figure 3.2. Stribeck diagram generated using method developed by Stanley and colleagues (1999). 42
Figure 3.3. Top piston ring friction force (red) and cylinder pressure trace (black).43
Figure 3.4. Second piston ring friction force per cycle.....44
Figure 3.5. Oil ring friction force per cycle. 44
Figure 3.6. Piston skirt friction force per cycle at 1000rpm. 45
Figure 3.7. Piston skirt friction force at 1000 rpm using μ=0.15 mPa-sec. 46
Figure 3.8. Typical journal bearing diagram showing key dimensions. 47
Figure 3.9. Rotating liner journal bearing friction force with liner rotation set to 3:1 reduction from crank speed. 48
Figure 3.10. Estimated baseline engine total instantaneous piston assembly friction per cycle at 1200 RPM. 49
Figure 3.11. Estimated RLE total instantaneous piston assembly friction force per cycle at 1200 RPM 50
Figure 3.12. Estimated average friction force of piston assembly. 51
Figure 3.13. Estimated parasitic torque of the rotating liner. 51

Figure 3.14. Comparison of models to Quad4 baseline and RLE measurements..53
Figure 3.15. Estimated fmep for the Cummins baseline and RLE. 54
Figure 4.1. Market application for heavy duty diesel engines (Peterson, 2016) ...57
Figure 4.2. Percent change in Global ship and boat building industry revenue (IBISWorld, 2016) 58
Figure A.1. Rotating liner partially inserted into engine block. 67
Figure A.2 Face sealing ring being inspected after engine disassembly. 67
Figure A.3. Head insert and recessed springs. 68
Figure 2.4. Rotating liner drive mechanism.....69
Figure A.5. Instrumentation setup of RLE testing.....70

CHAPTER 1: INTRODUCTION

1.A. Overview

Many modifications have been made to the original design of the internal combustion (IC) engine. These modifications have culminated into vast improvements in engine performance and efficiency. In the infant stage of its history, the main driving force for improvement was focused primarily on increasing efficiency and, thereby, overall torque output. Now in its current stage, increasing efficiency while decreasing emissions is the foremost necessity. This is due in large part to increasingly strict emissions policies and an inevitable rebound to inflated gas prices. As soon as next year an even higher tier of emissions standards will be implemented in the United States, and the need to generate new design solutions to accommodate those standards brings with it a new level of difficulty. Auto makers have already invested incredible amounts of resources to meet these challenges and will be required to continue to do so for the foreseeable future.

Chapter 1 will first overview the two main IC engine designs and the fundamental equations related to the efficiency of these designs. Then, historical use of the rotating sleeve valve engine will be outlined. Chapter 1 will conclude with prior research in IC engine frictional losses and the rotating liner technology. Chapter 2 describes the models used to estimate and compare the baseline and prototype engine. Chapter 3 pertains to the results of the models previously mentioned. Chapter 4 analyzes the commercial viability of the rotating liner technology. Finally, Chapter 5 offers conclusions and recommendations.

1.B. Back Ground

This section will cover the fundamentals of piston engine design to provide the reader with the necessary background needed to follow this report. The spark ignition engine and compression ignition engine are briefly described along with key efficiency equations pertaining to both. A summary of the historical use of the rotating sleeve valve engine is also presented.

1.B.1. The Spark Ignition Engine

The ideal thermodynamic cycle for the spark ignition engine is idealized as consisting of the four following processes:

1-2: Isentropic compression

2-3: Constant volume heat addition

3-4: Isentropic expansion

4-1: Constant volume heat rejection

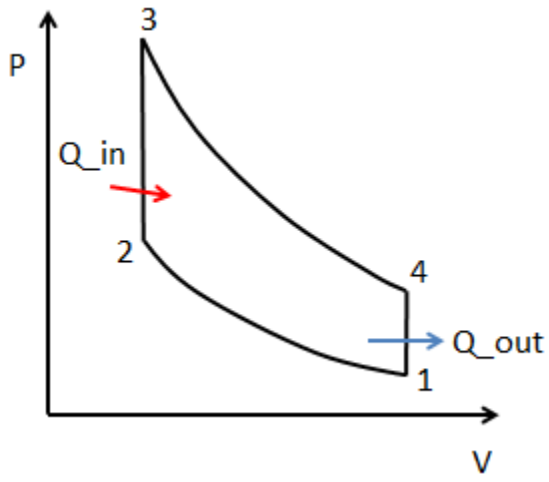

Figure 1.1. P-V Diagram of an ideal SI engine.

Like most ideal cycles, this oversimplifies the real-world process to such an extent it can be used mainly just to show correct trends of processes, but hardly estimates correct values for indicated thermal efficiency and brake power. Extensive modeling and experimentation has been done since the inception of the IC engine to find better correlations and modeling equations to real world engine characteristics. From this, three measurements are widely accepted as reasonable approaches to model engine performance; power, mean effective pressure, and specific fuel consumption.

$$bp = \eta_{ti}\eta_c\eta_v\eta_m\rho D\frac{N}{x}LHV_pFA_s \tag{1.1}$$

$$bmep = \eta_{ti}\eta_c\eta_v\eta_m\rho LHV_pFA_s\varphi \tag{1.2}$$

$$bsfc = \frac{1}{\eta_{ti}\eta_c\eta_m LHV_p} \tag{1.3}$$

where:

bp = Brake power $[\text{kW}]$

$bmep$ = Brake mean effective pressure $[\text{kPa}]$

$bfsc$ = Brake specific fuel consumption $[\text{g/kW-hr}]$

η_{ti} = Indicated thermal efficiency

η_c = Combustion efficiency

η_v = Volumetric efficiency

η_m = Mechanical efficiency

LHV_p = Constant pressure lower heating value of the fuel $[\text{kJ/kg fuel}]$

FAs = Stoichiometric fuel-air mass ratio $[\text{kg fuel/kg air}]$

ϕ = Fuel/air equivalence ratio

It is useful now to point out the difference between indicated power and brake power;

$$ip = \eta_{ti}\eta_c\eta_v\rho D\frac{N}{x}LHV_pFA_s\varphi \tag{1.4}$$

where:

$ip = \text{Indicated power } [\text{kW}]$

As can be seen by Equations 1.1 and 1.4, the only difference between indicated power and brake power is the inclusion of mechanical efficiency. Mechanical efficiency is the efficiency of converting the work available from the fuel throughout the thermodynamic cycle to work available at the output shaft of the engine. This efficiency is directly related to frictional and parasitic losses due to the various parts rubbing within the engine, which are described in detail later in this report, and due to the parasitic torque requirements, such as the oil pump, water pump, and alternator.

$$bp = ip - fp \tag{1.5}$$

Therefore, friction power can be accurately calculated by the difference between power at the top of the pistons (ip, from a P-V diagram and engine speed) and engine output shaft (brake power, bp). Overall friction power can, however, be experimentally approximated by hot motoring tests. Hot motoring is a procedure where the engine is connected to a motoring-capable dynamometer and warmed to operating temperature. The ignition system is then turned off and the throttle plate is held in the completely open positon, the amount of power needed to motor the engine using the dyno can be measured and interpreted as an approximation for the friction power.

1.B.2. THE COMPRESSION IGNITION ENGINE

The ideal thermodynamic cycle for a compression ignition (CI) engine is referred to as the Diesel Cycle. Instead of using a spark to ignite the fuel, Diesel engines compress the fuel-air during the compression stroke above the auto-ignition temperature of the fuel. In this cycle, the fuel injection process starts when the piston nears top dead center (TDC) during the compression stroke and continues during the first part of the power stroke. Figure 1.2 below, illustrates this cycle;

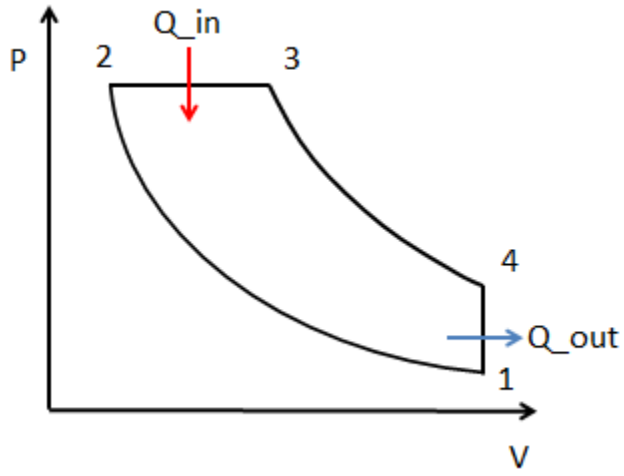

Figure 1.2. P-V Diagram of CI engine.

This key characteristic of Diesel engines allows the designed operating compression ratio to be much higher than in SI engines. The higher compression ratio coupled with diesel's higher constant pressure lower heating value (LHV_p) than gasoline provides improved thermal and overall efficiency over the SI engine. However, limitations in downsizing diesel engines while maintaining their efficiency benefits have not been fully overcome and therefore diesel engines have not become the dominant power plant for passenger vehicles in the U.S.

One draw-back worthy of being noted is that, in order to produce the high compression levels necessary in a diesel engine, many of the engine parts must be made to be more robust than their SI engine counterparts. This means heavier components and therefore reduced rotational speeds and increased inertial hindrances during transients. For reference, the average operating range for a semi-truck diesel engine is 500-3000 RPM. This will prove to be an opportunistic factor for rotational sleeve valve technology as this chapter explains engine frictional losses.

1.B.3. HISTORICAL USE OF ROTATING LINERS

In the early 1900's, traditional poppet valves used to be quite noisy and in any case, quite an undesirable noise to the consumer's ears. One solution to this problem was the invention of the sleeve valve engine. This design was created and patented by Charles Yale Knight, with his work on the design beginning in 1903. His "Silent Knight" proved to be much quieter than the poppet valve engines, but did not become a financial success in the United States. By mere chance Knight was able to present his engine to the British automaker Daimler, who became extremely interested in the design and, in turn, switched all production to these engines (Marshall, 2013). Daimler kept the Knight system in production up until the 1930's. Figure 1.3 below shows the general concept of the sleeve valve design;

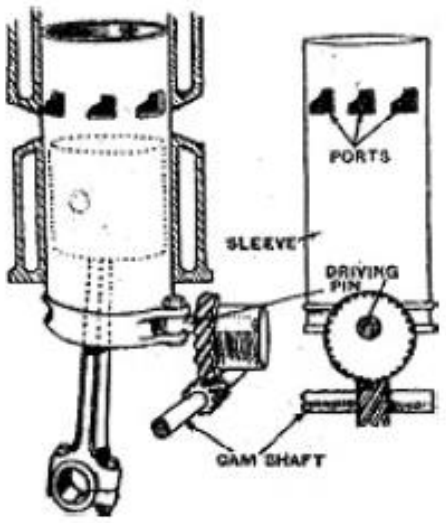

Figure 1.3. Sleeve valve engine design (Adams, 2010).

The sleeve valve engine replaced the poppet valves with inlet and exhaust vents that were bored through the sides of the cylinder walls, which were called the “sleeves” at the time of Knight’s invention but are more commonly called liners today, especially if they are removable from the engine during an overhaul (Adams, 2010). To open and close these vents, a rotatable cylinder sleeve was installed between the piston and the cylinder bore. The sleeve matched the length of the cylinder stroke and piston. The vent slots were placed in measured positions such that, when the cylinder sleeve is allowed to reciprocate in motion with the cylinder, as well as partially rotate, it opens passages to either the intake ports or exhaust ports during the correct times in the cycle which means the sleeve must reciprocate/rotate at half crankshaft speed. The motion of the cylinder sleeve is powered directly from the crankshaft.

Although the sleeve valve engine operated flawlessly, there remained drawbacks in the design. Since there was not a proper seal between the sleeve and the bore, relatively large amounts of oil could enter the combustion chamber during the intake

stroke. This caused the signature blue haze associated with Daimler automobiles powered by this engine.

Further development of the sleeve valve engine was produced by Sir Harry Ricardo starting in the early 1920's. Ricardo was tasked by the British Air Ministry to find a solution to more efficient aircraft engines either by improving the quite poor fuel quality being produced at the time, or by improving the conventional aircraft engine design. The sleeve valve engine was one option Ricardo and his colleagues decided to investigate and they observed multiple positive characteristics of their experimental sleeve valve engine. Among these characteristics, the sleeve valve showed absolutely no signs of engine knocking, compared to the baseline poppet valve engine, which was on the verge of knocking, and it showed a higher mechanical efficiency than the poppet valve baseline. After further research Ricardo concluded the sleeve valve engine could be designed robustly enough to give good performance at extremely high speeds, and to withstand long periods running at such speeds while under heavy loads (Marshall, 2013). These encouraging conclusions lead to the production phase of British aircraft utilizing sleeve valve engines by 1930.

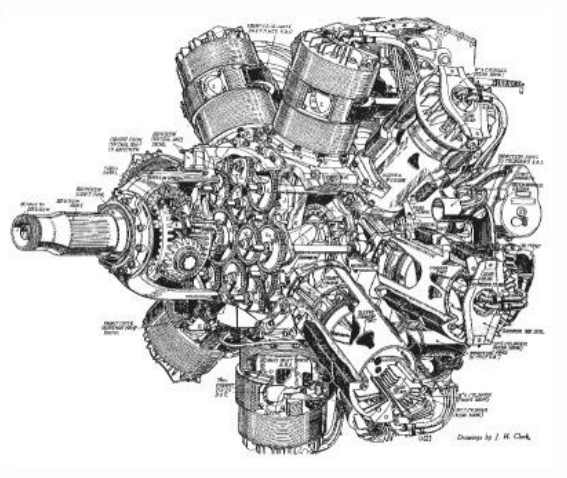

Figure 1.4. Bristol Hercules sleeve valve engine, http://www.sywellaerodrome.co.uk 2016.

1.C. Previous Research

This section provides information on piston engine mechanical friction losses and notable research that has previously been performed to analyze the subject. A well-known solution for reducing piston engine friction is also discussed in detail.

1.C.1. Frictional Losses Within Piston Engines

Modeling and reducing frictional losses within an IC engine are challenging research topics for piston engine technology. Frictional power consumption accounts for 10%-15% of the total available power extracted from the fuel at full load, 100% under no-load conditions, and a nonlinear function of load between these two extremes. Although 10%-15% does not seem like much, less than thirty percent of the fuel energy is converted to brake-torque and therefore any possible reductions in friction are well warranted in pursuing. Figure 1.5 outlines the distribution of the thermal energy extracted from the fuel in a conventional SI engine;

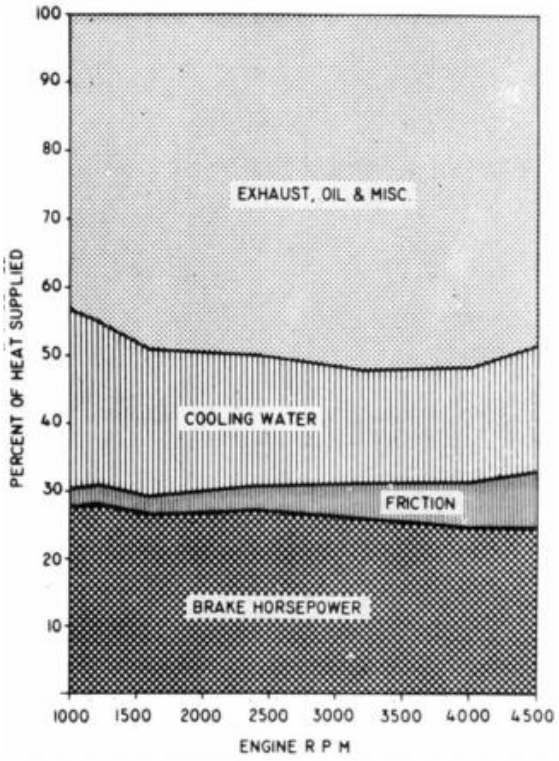

Figure 1.5. Distribution of thermal energy released by gasoline combustion for a homogeneous charge SI engine for one load condition, neglecting parasitic losses (Burke, Neglar, Campbell, and Lundstrom, 1967).

Further examination into the factors causing frictional torque losses has been an ongoing investigation with sometimes varying results (Sandoval and Heywood, 2003). It is widely accepted though, that the components causing an engine's internal frictional resistance can be grouped into the following three categories:

1. Crankshaft friction
2. Reciprocating friction (pistons and piston-rings)
3. Valve train

Early experimentation of components in these categories revealed the reciprocating friction to be significantly higher than the rest during all operating conditions (Cleveland and Bishop, 1960).

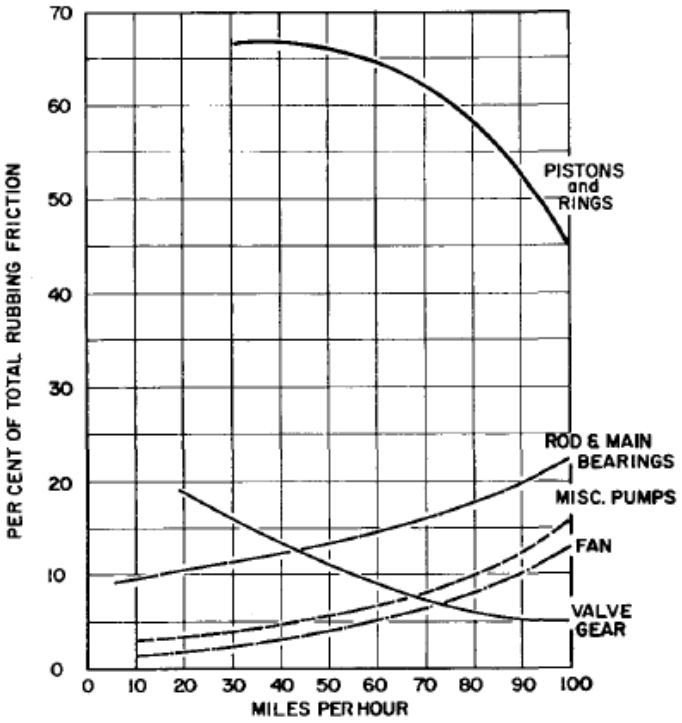

Figure 1.6. Early friction experimental results (Cleveland and Bishop, 1960).

In the years since this study, the exact portion to which each category contributes frictional losses has fluctuated due to variations in engine type, engine design factors, lubricants, models, and experiments. Nonetheless, it is still widely accepted that piston assembly friction dominates the other modes of frictional loss and that piston ring friction is highest at lower engine speeds.

Piston rings are a necessity for an IC engine to run properly and efficiently. The primary purposes of the piston rings are to seal the high-pressure combustion gasses from the crankcase and to prevent oil from entering the combustion chamber. Initial studies in piston and piston-ring friction noted several important observations, the first being that lubrication of the cylinder liner remained hydrodynamic except during the piston reversal events (TDC and BDC). They also noted that oil layer thickness increased with increasing engine speed and increasing oil viscosity, but decreased with increased engine

load. Lastly, they stated the predominant factors affecting piston ring friction are gas loading, number of rings, ring size, and ring design (Mcgeehan, 1978). Many studies and experiments have since been conducted to optimize piston ring design in order to reduce piston ring friction.

It is useful at this point to analyze the forces acting on the top piston ring in order to understand some of these early findings and the significance of these forces when developing piston-assembly related friction reduction solutions.

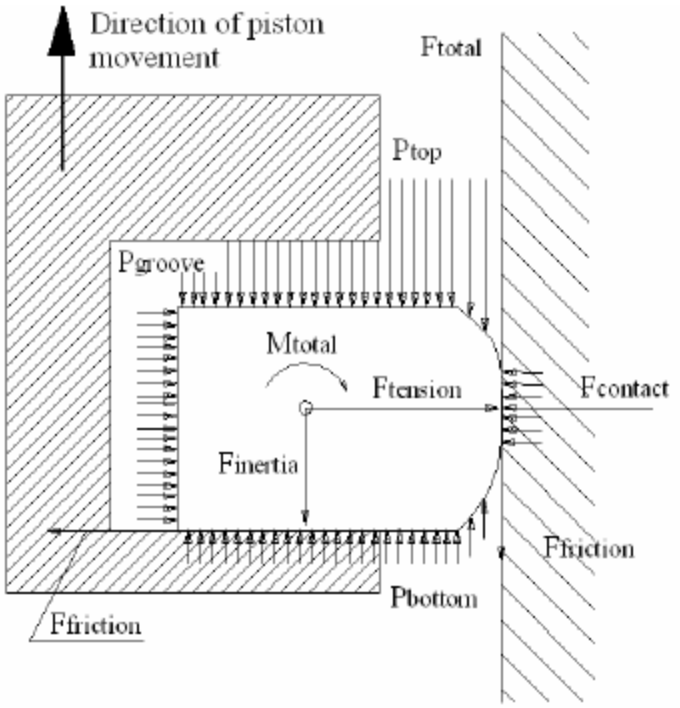

Figure 1.7. Forces acting on the top piston ring (Tamminen, Sandstrom, and Nurmi, 2005).

Figure 1.7 shows that the friction force (Ffriction) is a result of the normal force acting on the contact surface between the cylinder wall and the piston ring, Fcontact, where;

$$Fcontact = Pgroove \times A_{Ring\ contact\ surface} + Ftension \quad (1.6)$$

For reference, the pressure in the groove is relatively equal to or slightly lower than the in-cylinder pressures, which for a medium-duty diesel engine can reach upwards of 60 Bar. The top ring tension force can be estimated to be around 60 Newtons. When considering the contact surface area of the Cummins 4BT (the diesel engine selected for this experimentation) piston ring, the contact force exceeds 5800 N [1300 lb_f] at peak pressure. Although this magnitude of force exists only for a brief moment in piston cycle time, it is still very important to recognize that it exists, especially when examining the fluctuation in coefficient-of-friction the piston ring experiences during the engine cycle.

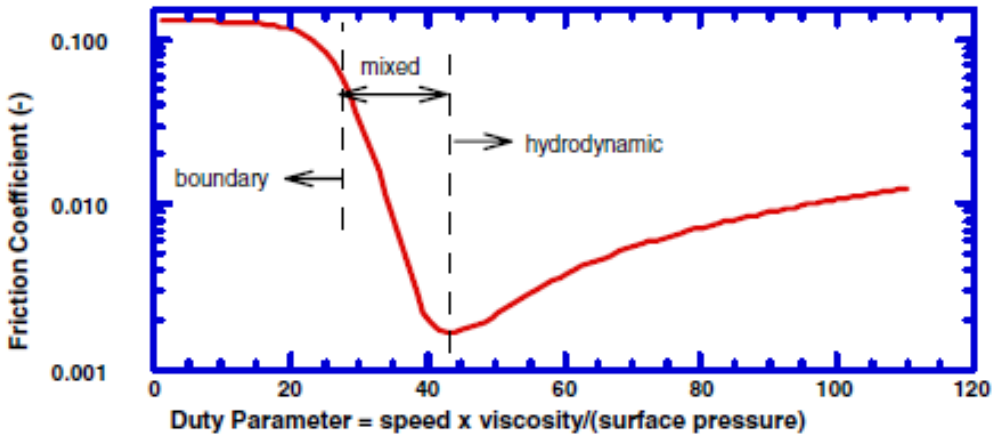

Figure 1.8. Stribeck diagram showing the regimes of friction for engine lubrication (Kim, Dardalis, Matthews, and Kiehne, 2005).

Figure 1.8 shows the piston rings operate over a wide range of friction coefficients, the highest range notably in the mixed lubrication and boundary lubrication regimes. When the piston reverses direction at top dead center (TDC) and bottom dead center (BDC) the piston rings are momentarily motionless, introducing a coefficient of friction upwards of 0.2 that is associated with the boundary lubrication regime. That is, the ring friction coefficient is 2-3 orders of magnitude higher near TDC of compression (when the cylinder pressure forcing the ring toward the liner is much higher than at any

other dead center) than the friction coefficient during hydrodynamic lubrication (the rings operate within the hydrodynamic lubrication regime throughout most of the stroke, and virtually all other sliding friction within the engine is also within the hydrodynamic regime).

Coupling the two aforementioned facts; the normal force acting on the top piston ring reaching magnitudes of 5800N at peak pressure and the coefficient of friction spiking at TDC, we can now estimate the maximum frictional force exerted on the top piston ring during this brief portion of the cycle.

$$F_{friction} = F_{normal} \times \mu = 5800 \times .2 = 1161\ N\ [\sim 225\ lbf] \tag{1.7}$$

Once the piston starts moving again, the piston ring migrates to operating within the hydrodynamic lubrication regime (less than one tenth the coefficient of friction in the boundary regime) and this piston ring friction force reduces rapidly.

1.C.2. Reducing Frictional Losses by Decreasing Oil Viscosity

The current, widely popular industry solution to reduce frictional losses and increase engine efficiency is to decrease the engine's oil viscosity. It should be stated this is not a new idea and has been the subject of research since the piston engine's early history. Though not new, it is still attractive because it is simple and the cost of implementation is vastly cheaper than researching other friction reducing methods. For these reasons, the gains in IC engine efficiency from reduced oil viscosity are examined in this section.

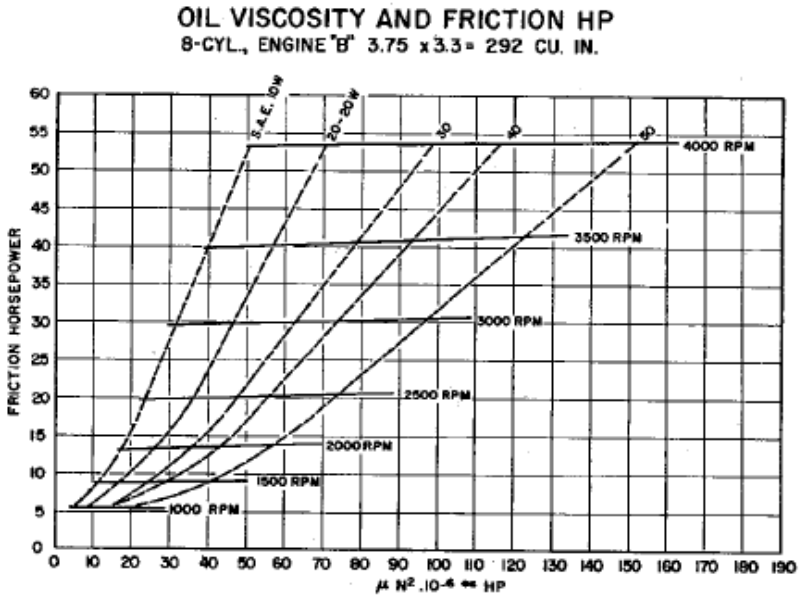

Figure 1.9. Effects of lowering oil viscosity (Cleveland and Bishop, 1960).

Figure 1.9 shows that auto manufacturers have long known that reducing oil viscosity will improve engine efficiency. During the period from about 1950 to 1975 fuel economy improvements between two and three percent were achieved in fully warmed up engines by a reduction in one SAE viscosity grade. Today, similar tests lowering the oil viscosity further reveal fuel economy improvements of less than one percent (Stanton, 2013).

Operating at increasingly lower oil viscosities starts to present some adverse effects that warrant attention. At TDC the oil film begins to break down, and at high temperatures can partially evaporate. In lower viscosity oil, abnormal and excessive wear begins to appear on the piston ring and TDC region of the cylinder. This is because with lower viscosity, less oil is retained in this region, thus causing a higher probability of direct metal-to-metal contact between the cylinder and piston ring. A secondary consequence of this low oil retention and possible evaporation is increased oil consumption (Permude and colleagues, 2012).

Studies seem to suggest the final limits in reducing oil viscosity are coming in the near future and that new ways must be looked at in reducing piston assembly friction. The following section describes the ongoing research to one such possible alternative; the rotating liner engine.

1.D. The Rotating Liner Engine

The rotating liner engine (RLE) was designed by Dr. Dimitrios Dardalis as a solution to reducing piston assembly friction by eliminating the conditions for which piston rings operate in the boundary lubrication regime. The RLE continuously rotates the cylinder liner during the combustion cycle to maintain a continuous motion between the piston/piston-rings and the liner. Thus, the relative sliding speed never approaches zero and therefore the duty parameter (x-axis) in the Stribeck diagram (Figure 1.8) never approaches zero and the piston assembly remains out of the boundary lubrication regime even near TDC of compression. The liner is rotated at a nominal speed to ensure that hydrodynamic lubrication is present even at the lowest ranges of engine RPM.

The first phase of this concept was tested for light-duty gasoline engines. Two 2.3L GM four cylinder Quad 4 engines were chosen for the experiment. The baseline was converted to run on only one cylinder just as the RLE prototype would. The original specifications of the engine are provided in Table 1.1.

Table 1. Baseline Engine Specifications

Type	Inline 4 cylinder
Displacement (L)	2.26
Stroke (mm)	85
Bore (mm)	92
Compression ratio	10:1
Intake valve opening	22° before TDC
Intake valve closing	45° after BDC
Exhaust valve opening	120° after TDC
Exhaust valve closing	20° after TDC

Table 1.1. Baseline SI Engine Specifications.

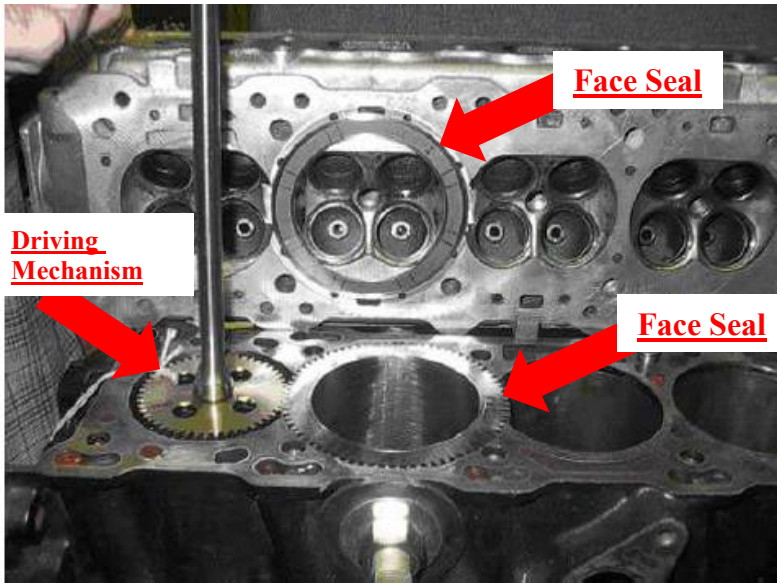

Figure 1.10. Alpha prototype RLE.

The three key components of the RLE, as shown in Figure 1.10, are the face seal, rotating liner, and liner drive mechanism. The face seal is a patented design created by Dr. Dardalis that is used to prevent combustion pressure leakage from occurring at the cylinder head and rotating liner interface while also minimizing oil leakage into the

combustion chamber. The driving mechanism for the rotating cylinder in this prototype was an electric motor to allow the effects of liner rotation speed to be examined.

Hot motoring experimental results showed positive results in friction reduction by cylinder rotation. Combustion pressure was also maintained through the patented face seal design. Friction power was measured to be between twenty-three and thirty-one percent lower in the RLE than the baseline, as shown in Figure 1.11. Tear down test results confirmed that the reduced frictional losses indeed were associated with the piston assembly.

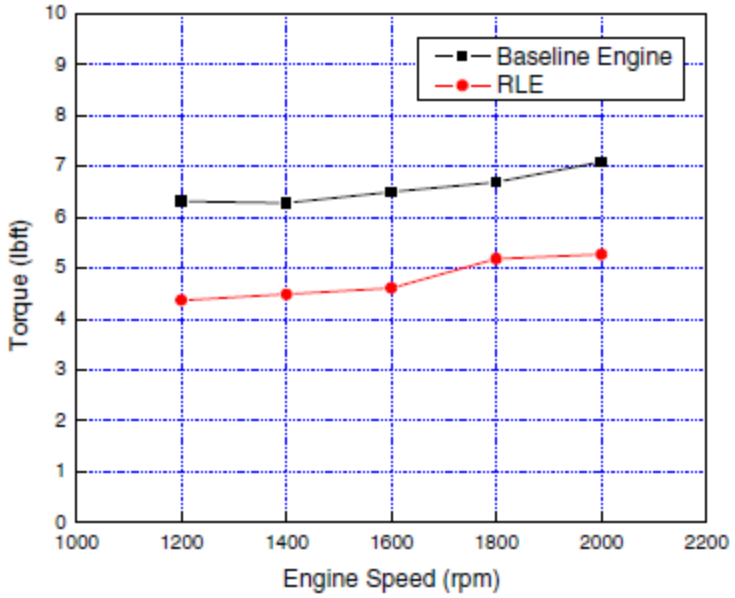

Figure 1.11. Baseline and RLE hot motoring friction torque measurements (Kim, Dardalis, Matthews, and Kiehne, 2005).

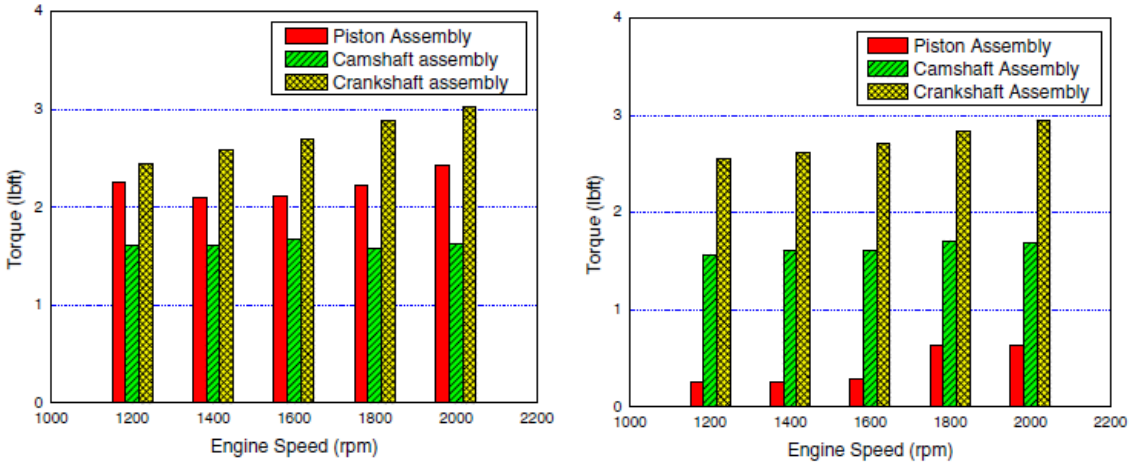

Figure 1.12. Tear down results of the baseline (left) and RLE (right) (Kim, Dardalis, Matthews, Kiehne, 2005).

Although the experiment succeeded in showing reduced piston assembly friction, there were discrepancies between the results and the predictive models used. The measured reductions in friction mean effective pressure (fmep) were substantially higher than the models predicted. These discrepancies at this time still cannot be explained by hard data, but possible theories were offered for the discrepancies (Kim and colleagues 2005). The models that were used are explained in Chapter 2.

CHAPTER 2: MODEL AND MODEL VERIFICATION OF ENGINE FRICTION AND FMEP

2.A. Overview

Modeling friction to predict fmep measurements is difficult due to the multiple nuances of moving components and range of operating lubrication regimes. There are multiple models that can be used to sum up and predict overall fmep, none of which are perfect so multiple ways will be covered to highlight advantages and disadvantages of the most commonly used models. It should be noted none of the models predicting overall fmep will be able to account for liner rotation, but nonetheless will render useful modeling results for predicting baseline fmep. However, instantaneous friction force models do account for varying friction coefficients during the engine cycle and therefore should provide reliable predictions in friction force reduction if it is assumed the liner rotation eliminates boundary lubrication during the piston reversal events. This chapter will first outline the initial fundamental piston assembly friction models that were created by Bishop (1964). Then, it will focus on the widely accepted model developed by Patton, Nitschke, and Heywood (1989) along with the updated models created by Sandoval and Heywood in 2003. A modified Patton, Nitschke, and Heywood model created by Shayler and Leong in 2005 is discussed afterward to highlight certain requirements that cannot be overlooked within the Patton, Nitschke, and Heywood model. Instantaneous piston friction models created by Stanley, Taraza, Henein, and Bryzik (1999) are discussed last to offer more precise guidance in predicting friction force reduction through liner rotation.

2.B. Models

There have been many attempts to model piston engine friction. This section will describe a few of the most well-known and widely accepted models for piston assembly fmep. Modifications and adjustments other researchers have made to these models are also explained.

2.B.1. THE FIRST FRICTION MODELS DEVELOPED BY BISHOP

Bishop (1964) was the first to generate a detailed model for the contributions of individual engine components to total fmep. He divided the mechanical friction into three main losses: piston mechanical friction, crankcase mechanical friction (journal bearing friction, valve gear friction, and pump and miscellaneous friction), and various types of pumping loop losses that will not be discussed further. Bishop divided piston friction into two main categories: viscous (piston skirt) and nonviscous (ring friction forces due to ring tension and gas pressure forces behind the ring). He decided that the ring friction was nonviscous because it was not sensitive to engine speed, from tests using a CFR engine, but it is worth noting that the CFR has a very limited range of engine speeds and has very high frictional losses in the valve train. For piston skirt "and ring" viscous friction, he needed a size parameter for which he picked the projected area of the skirt, $L_{skirt,eff}$, divided by the product of the bore and stroke. Further, he defined the effective piston skirt length as the projected area of the skirt divided by the bore, which he said was ~2 inches (~50 mm) for most passenger car engines at that time. Thus:

$$\begin{aligned} \text{fmep}_{\text{piston skirt}} &= \frac{\mu_{oil} A_{shear} N \cdot S_p}{\frac{\pi}{4} B^2 S \cdot N} \\ &= 21.93 \frac{L_{skirt,eff}}{B \cdot S} \left(\frac{2S \cdot N}{1000} \right) \end{aligned} \tag{2.1}$$

where:

μ_{oil} = Dynamic viscosity of oil

S_p = Piston speed

A_{shear} = Piston side shearing area

N = Engine speed

B = Bore

S = Stroke

$L_{skirt,eff}$ = Effective skirt length

The constant has the dynamic viscosity of the oil (μ_{oil}) embedded within it. He assumed the piston speed (S_p) was proportional to the mean piston speed (2SN). He also assumed that A_{shear} is proportional to the product of the bore and the effective length of the skirt. For the nonviscous ring friction due to ring tension, he used:

$$\begin{aligned} fmep_{ring\ tension} &= \frac{F_{f,tens}\Delta x_p N}{\frac{\pi}{4}B^2 S \cdot N} n_{rings} = \frac{F_{f,tens}\left(S_p(\theta)\Delta\theta\right)}{\frac{\pi}{4}B^2 S} n_{rings} = \frac{F_{f,tens}\left(S_p(\theta)/N\right)}{\frac{\pi}{4}B^2 S} n_{rings} \\ &= \frac{F_{f,tens}\left(2S\cdot N/N\right)}{\frac{\pi}{4}B^2 S} n_{rings} = 2.11\frac{S}{B^2} n_{rings} \end{aligned} \quad (2.2)$$

where:

$F_{f,tens}$ = Friction force due to ring tension

θ = Crank angle

n_{rings} = Number of rings

Bishop replaced the instantaneous piston speed with the mean piston speed, and replaced the change in crank angle with the inverse of the engine speed, and the constant in his final expression combines several constants and the friction force (which is also constant in the boundary lubrication regime but not in the mixed or hydrodynamic lubrication regimes) to yield Equation 2.2. For the nonviscous ring friction due to gas pressure behind the rings, Bishop used:

$$\text{fmep}_{\text{ring gas pressure}} = \frac{\text{MAP}}{\text{p}_\infty} 2.35 \frac{\text{S}}{\text{B}^2} \left(0.088\text{r}_\text{c} + 0.182\text{r}_\text{c}^{\left[1.33 - \frac{0.121\text{S}_\text{p}}{1000}\right]} \right) \tag{2.3}$$

where:

MAP = Manifold absolute pressure

r_c = Compression ratio

Bishop offered little justification for the relationships in this equation.

2.B.2. PATTON, NITSCHKE, AND HEYWOOD MODELS

Patton, Nitschke, and Heywood originally developed individual friction models based off of Bishop's models for each category of friction producing components in 1989 (Patton, Nitschke, and Heywood 1989). These models provide a basis for reliably predicting frictional power losses and FMEP in IC engines. They also confirmed that reciprocating friction accounts for the greatest amount of torque losses at lower engine speeds, and show this friction is due foremost to boundary lubrication.

As discussed in the original paper by Patton, Nitschke, and Heywood (1989), there are three terms governing the piston and piston-ring friction model. The first is the "piston friction term", which is more precisely the piston skirt friction term and was derived from the friction coefficient for hydrodynamic lubrication, piston skirt length, and piston velocity.

$$F_{f,piston\ skirt} = fF_n \propto \frac{\mu V L_s F_n}{F_n} \propto VL_s \propto S_p B \times constant \tag{2.4}$$

$$P_{f,piston\ skirt} \propto F_{f,piston\ skirt} V \propto S_p^2 B \tag{2.5}$$

$$fmep_{piston\ skirt} \propto \frac{P_f}{NV_d} \propto \frac{S_p^2 B}{B^2 SN} = \frac{S_p^2 B}{B^2 S_p} = \frac{S_p}{B} \times constant \tag{2.6}$$

where:

f = Friction coefficient

F_n = Normal force acting on cylinder wall

L_s = Piston skirt length

V = Piston velocity

V_d = Displaced volume

After proving fmep is proportional to mean piston speed and bore size, Patton, Nitschke, and Heywood (1989) established an empirical constant through data measurements of two hot motored engines, this constant was found to be $2.94\times 10^2 \frac{kPa-mm-s}{m}$. Sandoval and Heywood (2003) revised this term to account for oil viscosities other than the original type used in finding the empirical constant. The final relationship for piston fmep is;

$$fmep_{Piston\ skirt} = 2.94\times10^2 \left(\sqrt{\frac{\mu}{\mu_0}}\right)\left(\frac{S_p}{B}\right) \tag{2.7}$$

where:

μ = Dynamic viscosity of oil used

μ_0 = Originally used dynamic viscosity of oil

The next term accounts for piston ring friction without gas loading, i.e. the normal force exerted on the cylinder wall created by the tension of the piston ring. As with the piston friction term, an emperical constant was found for this term as well. The original model is as follows:

$$F_{f,ring\ tens} = fF_n \propto \left(1+\frac{1000}{N}\right)\times constant \tag{2.8}$$

$$P_{f,ring\ tens} \propto F_{f,ring\ tens}V \propto \left(1+\frac{1000}{N}\right)S_p \tag{2.9}$$

$$fmep_{ring\ tens} \propto \frac{P_f}{NV_d} \propto \left(1 + \frac{1000}{N}\right)\frac{S_p}{NB^2S} = \left(1 + \frac{1000}{N}\right)\frac{1}{B^2} \tag{2.10}$$

$$fmep_{ring\ tens} = 4.06\times10^4 \left(1 + \frac{1000}{N}\right)\frac{1}{B^2} \tag{2.11}$$

Three modifications have since been implemented to enhance this model; these are to account for the lower tension and smoother surface finishes of modern piston ring designs. Due to the wide variation among piston ring designs and surface finishes, these two factors must be measured experimentally for each individual engine. The third modification lessens the rate of decay seen by the term at increased RPM.

$$fmep_{ring\ tens} = 4.06\times10^4 \left(\frac{F_t}{F_{to}}C_r\right)\left(1 + \frac{500}{N}\right)\frac{1}{B^2} \tag{2.12}$$

where:

C_r = Piston roughness constant

F_t / F_{to} = Piston ring tension ratio

The final term accounts for the friction made by the piston ring due to gas pressure loading.

$$fmep_{gas\ load} = 6.89\frac{P_i}{P_a}\left[.088r_c + .182r_c^{\left(1.33-.028S_p\right)}\right] \tag{2.13}$$

where:

P_a = Atmospheric pressure

P_i = Intake manifold pressure

This term was orignally found by Bishop (1964) using emperical analysis and later converted into metric terms by Patton, Nitschke, and Heywood (1989). Again, Sandoval and Heywood (2003) updated this term to account for different oil viscosities, improved piston ring designs, and liner surface polishing.

$$fmep_{gas\ load} = 6.89\frac{P_i}{P_a}\left[.088\left(\sqrt{\frac{\mu}{\mu_0}}\right)r_c + .182\left(\frac{F_t}{F_{to}}\right)r_c^{(1.33-.028S_p)}\right] \quad (2.14)$$

It should be noted that in the papers referenced throughout this section, there is a fourth term associated to form the overall recriprocating friction model which accounts for the connecting rod bearings. Since this term is not affected by a rotating cylinder liner it is not examined at length in this report, but is given below in its updated form for later reference (Sandoval and Heywood, 2003).

$$fmep_{rod\ bearing} = 3.03\times10^{-4}\sqrt{\frac{\mu}{\mu_0}}\left(\frac{ND_bL_bn_b}{B^2Sn_c}\right) \quad (2.15)$$

where:

D_b = Bearing diameter
L_b = Bearing length
n_b = Number of bearings
n_c = Number of cylinders

Hot motoring experimentation with 3.0 L and 5.4 L engines confirmed that the total reciprocating assembly friction model (without gas loading) accurately matches emperical results up to 2500 RPM. However, depending on the engine displacement, the model diverges more from the results in the mid to high range RPM as shown in Figure 2.1. Gas loaded piston friction is particularly hard to measure with current technologies and in the papers discussed was omitted in their experimental results.

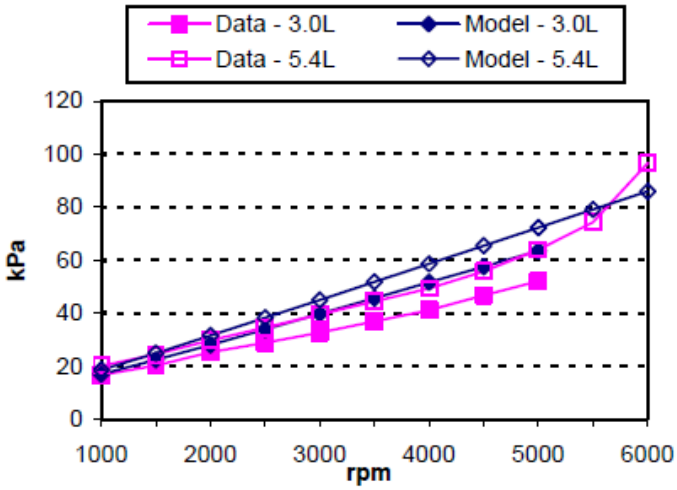

Figure 2.1. Experimental results compared to model predictions for reciprocating piston friction (Sandoval amd Heywood, 2003)

2.B.3. SHAYLER, LEONG, AND MURPHY MODIFICATIONS TO THE PATTON, NITSCHKE, AND HEYWOOD MODELS

The friction models outlined in the previous section will be useful for future testing of the RLE and baseline engines, but are difficult to utilize without a few modifications. The 2003 updates provide a basis for the adjustments by recognizing modern optimized design parameters and varying oil viscosities. However, the experimental constants found for each equation can only apply to engines similar to that used in the papers and new constants must be generated for various engine types. According to Meloni and Cacciatore (2013), the scaling terms must be calibrated with new constants obtained from experimental data for the specific engines being tested. Calibrating was also performed by Shayler, Leong, and Murphy (2005) during their experimentation by running tests and using constants that best correlated model trends with their data. Furthermore, Shayler, an colleagues observed that the piston and piston-skirt are weighted by mid-stroke conditions similar to those for hydrodynamic slipper bearings, and therefore declared a dependence on $S_p^{0.5}$ rather

than S_p. Shayler and colleagues provided tables for their adjusted constants along with the modified equations. The modified equations and values of the constants are shown below;

$$fmep_{pistonskirt} = C_{ps}\left(\frac{V_p^{.5}}{B}\right)\left(\frac{\mu}{\mu_0}\right)^n \tag{2.16}$$

$$fmep_{ringtens} = C_{pr}\left(\frac{V_p^{.5}}{B^2}\right)\left(\frac{\mu}{\mu_0}\right)^n \tag{2.17}$$

$$fmep_{rodbearing} = C_{pb}\left(\frac{N^{.6}D_b^3 L_b n_b}{B^2 S n_c}\right)\left(\frac{\mu}{\mu_0}\right)^n \tag{2.18}$$

where:

V_p = Mean piston speed

$C_{ps} = 14.0$

$C_{pr} = 2707$

$C_{pb} = .0202$

Shayler, and colleagues leave the "gas pressure loading" term out of their analysis. They justify this by comparing hot motoring data from when the engine is fully assembled and maintaining pressure during the engine cycle (without firing) to motoring data from when the engine is adapted to allow the cylinders to remain decompressed during the engine cycle. The data comparison revealed similar values for both instances, from which they deduced that the "gas pressure loading" term had considerably less effect than Patton, Nitschke, and Heywood predicted (Shayler, Leong, and Murphy 2005). While neglecting this term may be possible during hot motoring tests, where pressures are considerably lower than when fuel ignition occurs during engine firing, this

is highly unlikely during actual operating conditions (engine firing). Evidence supporting this last statement is outlined in the next section, where frictional forces dependent on gas loading and crank angle are discussed.

2.B.4. STANLEY, TARAZA, HENEIN AND BRYZIK SIMPLIFIED PISTON ASSEMBLY FRICTION MODEL

The Patton, Nitschke, and Heywood models are highly useful, but only model average fmep over engine speed and cannot be related to instantaneous piston friction. To accurately predict the benefits of the rotating liner piston assembly, friction must be examined on a crank angle dependent basis. Rezeka and Henein (1984) developed fundamental equations to model instantaneous piston friction which have since been widely used and improved upon (Stanley, Taraza, Henein, and Bryzik 1999). This section will focus on the simplified models for the piston rings and piston skirt created by Stanley and colleagues (1999).

A critical part in modeling instantaneous piston friction is determining the friction coefficient between the piston rings and the cylinder wall. Figure 2.2 shows a simplified Stribeck curve.

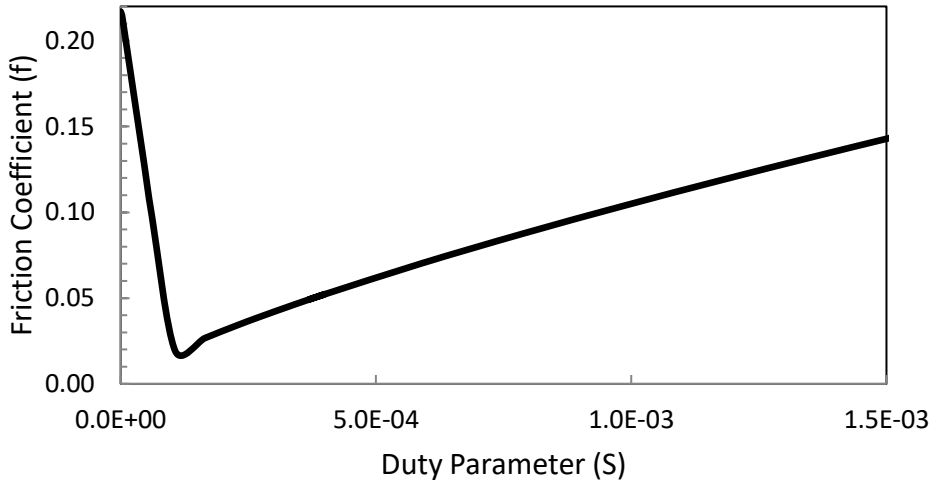

Figure 2.2. Simplified Stribeck diagram.

The Stribeck diagram generally relates the friction coefficient between two journal bearing surfaces to the dimensionless Sommerfeld Number (or "bearing characteristic number"). It is defined as the radial clearance ratio squared times the dynamic viscosity of the oil between these two surfaces times the rotational speed divided by the load (force) per unit of projected bearing area. Ting (1993) modified the Sommerfeld Number for the specific case of piston rings by replacing the rotational speed with the ratio of the sliding velocity to the ring width. Ting did not discuss what to do about the radial clearance ratio term appearing in the Sommerfeld Number but it is common practice to both ignore this term in the x-axis parameter on graphs of the friction coefficient and to simply call the independent variable the duty parameter instead of a modified Sommerfeld Number.

Equation 2.19 defines the duty parameter (the x-axis) to show its dependencies and, consequently, the dependencies of the piston ring friction coefficient.

$$S = \frac{\mu \left| S_p \right|}{P \cdot L_i} \tag{2.19}$$

where:

L_i = Active height of ring profile

Sui and Ariga (1993) solved the Reynolds and force equilibrium equations simultaneously to examine the effects of ring surface topology on piston ring pack friction and ring lubrication. They initially validated their model against measurements from a moving liner test rig and then used their model to simulate ring pack friction under engine firing conditions. They distinguished between the three regimes of lubrication (hydrodynamic, mixed, and boundary) using a dimensionless oil film thickness parameter, Λ, defined as:

$$\Lambda \equiv \frac{h}{\sigma} \tag{2.20}$$

where h is the nominal oil film thickness and σ is the composite surface roughness. They stated that "It is generally understood that, for $\Lambda < 1$, the lubrication mechanism is operated in boundary lubrication regime due to the severe involvement of asperity contacts, and is in pure hydrodynamic regime for $\Lambda > 6$ since the influence of surface roughness is insignificant. For Λ within 1 to 6, it is referred to as the mixed lubrication since the surface roughness is involved with the hydrodynamic motion. Asperity interlocking normally occurs when Λ is less than 4." Among their findings were: 1) the surface roughness pattern has a very substantial impact on ring pack friction; 2) this friction reduction results from an increase in film thickness, and 3) the oil control ring friction is the most sensitive to surface roughness. Regarding the last finding, they determined that oil film thickness parameter varied from ~2.5 near TDC to 45 at mid-stroke for the top ring whereas it varied from 1.4 to 4 for the oil control ring.

Stanley and colleagues noted that piston ring curvature heavily influenced the dependency of the friction coefficient on the duty parameter and so developed a method

for creating unique Stribeck curves for varying piston ring curvature (Stanely, et al. 1999). Figure 2.3 shows the typical ring curvatures (along with critical dimensions) of each piston ring.

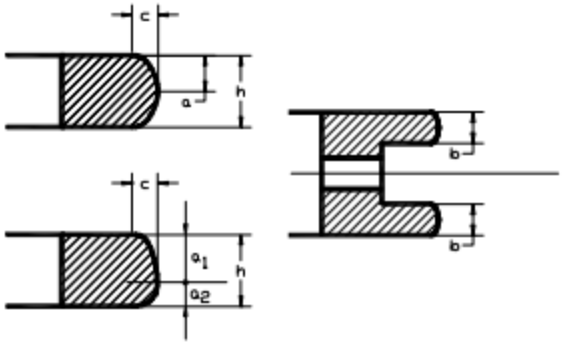

Figure 2.3. Top ring (top left), second ring (bottom left), and oil ring (middle right) curvature profiles (Taraza, Henein, and Bryzik 2000).

The hydrodynamic lubrication regime is estimated by the relationship of a logarithmic function;

$$f = C \times S^m \tag{2.21}$$

where C and m are functions only of the curvature of the ring profile "c/a" (Stanley, et al. 1999). Figure 2.4 was generated by Stanley and colleagues (1999) to find C and m. When varying values of "c/a" it is noted to have substantial effect on the piston ring friction coefficient. If there is a large amount of curvature in the ring profile, there is increased lubricant "wedge action" which promotes hydrodynamic lubrication (therefore reducing friction) during the mid-stroke of the piston cycle. The large amount of ring curvature conversely has a negative impact on the "squeeze film" effect, lowering lubricant pressure (therefore increasing friction) near the dead centers of the cycle (Jeng, 1992). A flat ring profile has the opposite results, meaning higher friction during mid-stroke due to less "wedge effect" and lower friction during piston reversal events due to an increase in the "squeeze film" effect (Jeng, 1992).

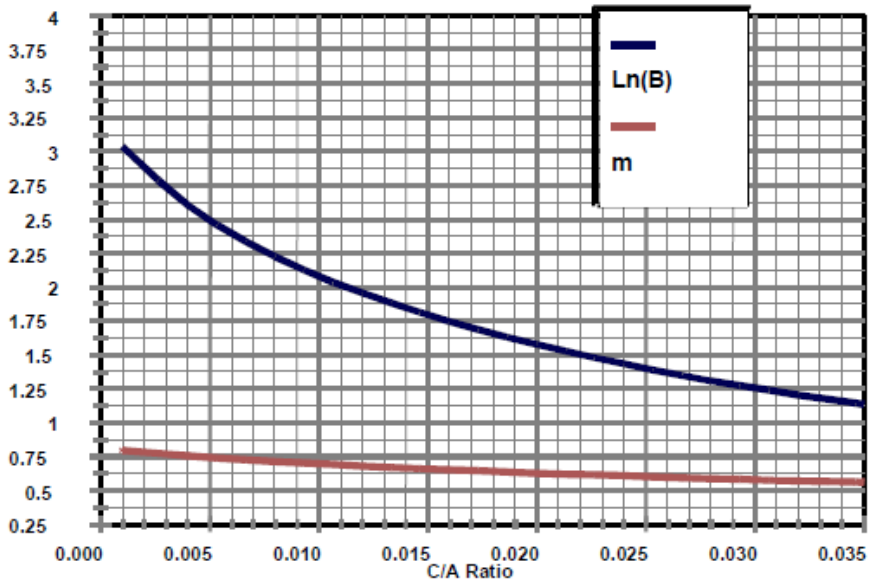

Figure 2.4. Stribeck coefficients (Stanley, et al. 1999).

The transition from hydrodynamic to mixed lubrication happens at the critical duty parameter (S_{cr}). Since S_{cr} is not readily measurable, Stanley and colleagues suggest that a reasonable assumption based on typical oil film behavior and ring and liner asperity height is $S_{cr} = 1 \times 10^{-4}$. For mixed lubrication, a linear relation was created (Stanley, et al. 1999);

$$f = f_0\left(1 - \frac{S}{S_{cr}}\right) + f_{cr}\left(\frac{S}{S_{cr}}\right) \tag{2.22}$$

where:

$f_0 =$ Friction coeffient of metal-to-metal contact

A moderate assumption for the friction coefficient of metal-to-metal contact is $f_0 = 0.22$ (Stanley, et al. 1999) (Xu, et al. 2005) . Although the boundary lubrication regime is entered momentarily, it still has a significant impact on the friction force acting on the piston ring, and therefore needs to be accounted for. Stanley and colleagues (1999)

state that the duty parameter enters the boundary regime at $S_B \approx 1.0\times10^{-10}$. This provides a simple equation for the final portion of constructing the Stribeck diagram;

$$f = f_0 \quad \text{For: } S \le S_B \tag{2.23}$$

Once the Stribeck curve is created using Equations 2.21, 2.22, and 2.23 the frictional force for each piston ring can be calculated based on the cylinder pressure and piston speed. Taraza and colleagues (2000) noted the oil starvation process needs to be accounted for when calculating the friction force of each piston ring. The oil starvation process is defined by the oil film thickness that is available for a certain ring in the ring pack, which is linked to the minimum oil film thickness left behind from the preceding ring (Taraza, et al. 2000). This is accounted for in the duty parameter by the "active height of ring profile" term. The first ring has an active length of $L_1 = 0.25a$, the second ring has $L_2 = 0.25a_1$ (for upstroke) or $L_2 = a_2$ (for downstroke), and the oil ring has $L_3 = 2b$, where a, a_1, a_2, and b are the dimensions found in Figure 2.3 (Taraza, et al. 2000).

Piston skirt friction forces are just as complex to model as piston ring friction forces. In order to create a model for instantaneous piston skirt friction Stanley and colleagues (1999) made a few assumptions and simplifications. These assumptions were (1) the skirt is fully engulfed in oil from the oil entrance point to the oil exit point (no cavitation), (2) a Newtonian lubricant is used, so the Reynold's equation applies, (3) thermal and elastic deformation of the skirt and liner are neglected, and (4) purely hydrodynamic lubrication is considered (Stanley, et al. 1999). They simplified the model such that only a few key parameters are needed in order to obtain piston skirt friction forces;

$$F_{f,pistonskirt} = Fcp \times \mu \times a \times S_p \tag{2.24}$$

where:

Fcp = A constant correlated to cylinder bore and skirt dimensions

a = skirt shearing length

Fcp is found using Figure 2.5 generated by Stanley and colleagues (1999) and the piston skirt characteristic parameter Scp;

$$Scp = \frac{\left(\frac{D-d}{2}\right)^{\frac{7}{8}} \cdot c^{\frac{1}{8}}}{\pi \cdot D} \tag{2.25}$$

where:

D = Cylinder bore

d = Maximum piston skirt diameter

c = Skirt recess length

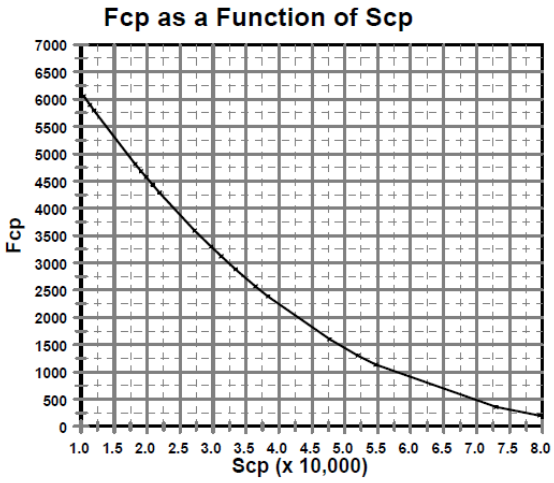

Figure 2.5. Fcp as a function of Scp (Stanley, et al. 1999).

The skirt recess length (c) refers to the difference in diameter of the top of the piston skirt to the maximum diameter around its mid-point. The skirt recess length is very small and is usually around 0.1 mm. The skirt shearing length (a) refers to the length from the top of the piston skirt to the maximum skirt diameter. The dimensions are

defined in the same manner as the top piston ring dimensions, c and a, and for visual clarification can be referred to in Figure 2.3.

Instantaneous imep method experiments (explained in detail in the original paper) were performed to validate the models outlined in this section using a single cylinder Deutz diesel engine. Figures 2.6, 2.7, and 2.8 show their results and that model trends match their data;

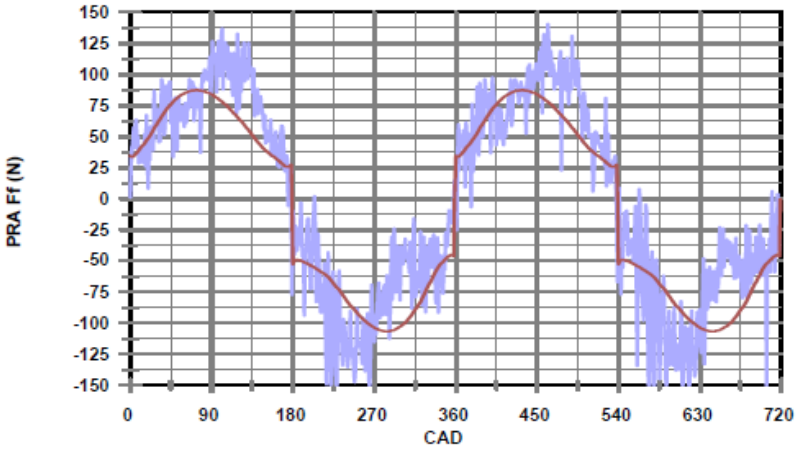

Figure 2.6. Piston ring assembly friction model (red) vs. experiment (blue); 500 RPM, motored, no head (Stanley, et al. 1999).

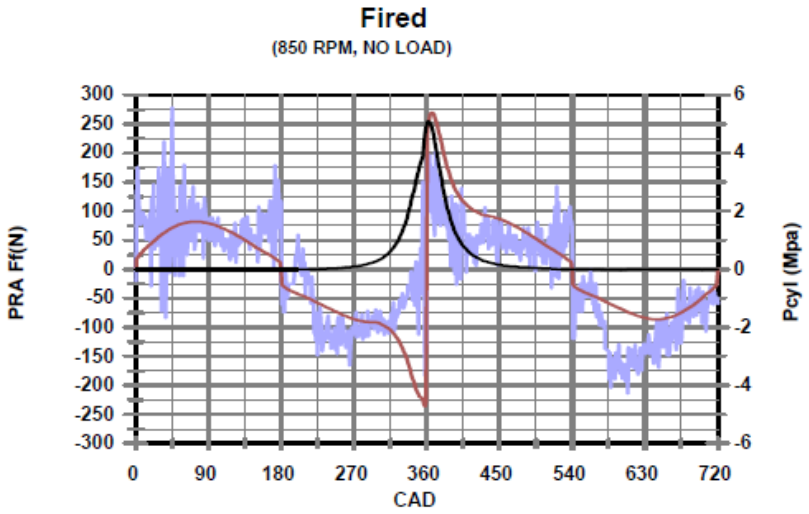

Figure 2.7. Pisont ring assembly friction force (fired, no load) model (red) vs. experiment (blue), 850 RPM (Stanley, et al. 1999).

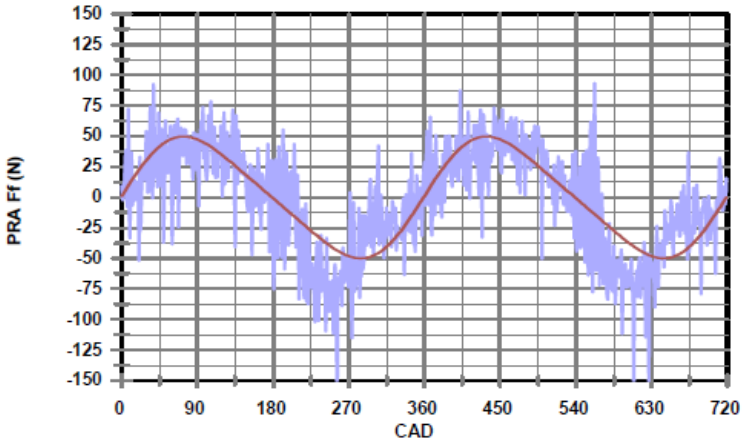

Figure 2.8. Skirt friction model (red) vs experiment (blue); 500 RPM, motored, no head (Stanley, et al. 1999).

Although some discrepancies can be seen between the piston ring assembly friction model and the firing data (shown in Figure 2.7) Stanley and colleagues determined the models are valid and that (1) hydrodynamic lubrication occurs during the middle of each of the four strokes and (2) mixed lubrication occurs at the dead centers and more significantly at firing TDC (Stanley, et al. 1999). Their second statement seems to lack any mention of boundary lubrication at the dead centers. This is somewhat problematic since it is generally accepted otherwise that boundary lubrication is present

at the dead centers. Nonetheless, these models will prove useful in estimating the frictional torque encountered by the rotating liner during the engine cycle as discussed in the next chapter.

It is worth pointing out that the poor agreement between the model and data for firing operation at a low engine speed could be due to neglecting the boundary lubrication regime. At low engine speed, their neglect of the squeeze film effect may have decreased the error in their neglect of the boundary lubrication regime.

CHAPTER 3: FRICTION TORQUE AND FMEP ESTIMATION

This chapter shows the implementation of the models discussed in Chapter 2 to estimate piston assembly friction forces and fmep of the heavy-duty diesel baseline and RLE engines. The piston assembly friction forces are individually calculated and summed afterward. Friction forces attributed to the rotating liner journal bearings and face seal are calculated as well to estimate possible rotating liner parasitic torque values. The Patton, Nitschke, and Heywood (1989) model and the modified Shayler, Leong, and Murphy (2005) model are compared to fmep measurements found during the Quad 4 gasoline baseline and RLE experimentation. The two models are then used to predict fmep of the heavy-duty diesel baseline and RLE engines. Table 3.1 shows the parameters of the engine used for the model.

Cummins 4BT Engine Parameters		
Bore	102	[mm]
Stroke	120	[mm]
Crank Throw	59.64	[mm]
Rod Length	192.16	[mm]
Main Bearing ID	50.8	[mm]
Main Bearing Width	25.4	[mm]
Top Ring Height	2.8	[mm]
Second Ring Height	2.75	[mm]
Oil Ring Contact Height	1.56	[mm]
Skirt Shearing Length	35	[mm]
Skirt Recess Length	0.1	[mm]
μ_oil (10W-30 @75C)	0.02	[Pa-s]
Top ring tension	70	[N]
Second Ring tension	60	[N]
Oil Ring Tension	80	[N]

Table 3.1. Cummins 4BT engine parameters

The bore and stroke were determined by referring to the Cummins 4BT manual and can also be found through multiple sources on the web. The crank throw, rod length, bearing dimensions, and skirt parameters were found using SolidWorks models of the piston, rod, and crank. The ring tension values were estimated based on values given by Stanley and colleagues (1999) and Rakapoulos and colleagues (2002).

3.A. Rotating Liner Torque Estimation

This section will first use the instantaneous piston friction model developed by Stanley and colleagues (1999) to estimate the Cummins baseline engine piston assembly friction. It will then apply these methods to the Cummins RLE. Finally, summing the RLE piston assembly friction along with the additional friction contributions associated with the rotating liner will then be utilized to estimate the torque to rotate the liner.

3.A.1. Piston Ring Assembly Friction Contribution

Using the process outlined by Stanley and colleagues (1999), the first step to finding the instantaneous friction force of the piston rings is to calculate the duty parameter and friction coefficient for the entire cycle for each piston ring. Crank angle, cylinder pressure, oil viscosity, and piston ring dimensions are required to perform these initial calculations. The parameters of the engine used for the model are found in Table 3.1. Figure 3.1 is an example pressure trace that was used in the model.

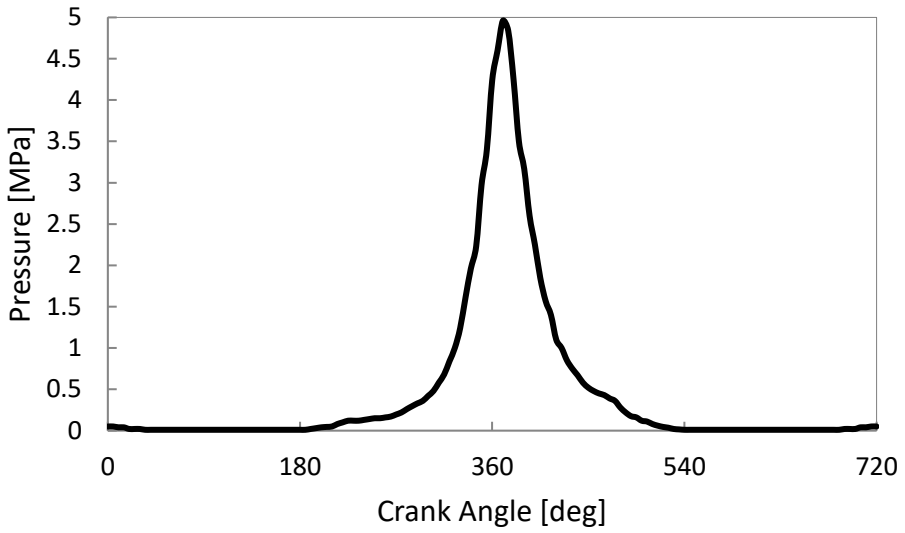

Figure 3.1. Pressure trace of a heavy-duty diesel engine at 1000 rpm with no load.

Using Equations 2.19, 2.20, and 2.21, a Stribeck diagram can be created for a specific engine. For Equation 2.20, the ring curvature profile needs to be determined in order to find the corresponding constants on Figure 2.4. This could not be measured accurately due to the minimal length of the ring profile curvature (C). However, Stanley and colleagues used a similar diesel engine in their experiment and used C/A= 0.001. Values for C/A were varied from 0.001-0.005 to determine if it had a significant effect on the overall results. The change in results was less than 1% and so a C/A value of .001 was chosen considering the similarity in engine type and age between the Cummins 4BT and the engine used by Stanley and colleagues (1999). Figure 3.2 shows the Stribeck diagram corresponding to the Cummins 4BT. It should be noted the boundary lubrication regime is present in Figure 3.2, but due to the extremely small duty parameter values Stanley and colleagues state are associated with boundary friction, $S=1\times10^{-9}$, it is hardly visible in the figure.

Figure 3.2. Stribeck diagram generated using method developed by Stanley and colleagues (1999).

Using Equation 1.6, Equation 1.7, and Figure 3.2, the friction forces of the piston rings were calculated over the full engine cycle. Figure 3.3 shows the top piston ring friction force overlaid by the cylinder pressure. There are several interesting features to take note of in Figure 3.3. The first is the maximum magnitude of the friction force around TDC of the compression stroke. This value can be found by doing a simple hand calculation and makes for an easy check to see if the model has the correct form and inputs. The second feature of interest is the three remaining piston reversal points. As expected, at each dead center there is boundary lubrication which is seen by the rapid increase of friction force which then changes sign as the piston reverses direction. The final interesting features are the mid stroke regions which show logical trends that correlate to a hydrodynamic lubrication regime.

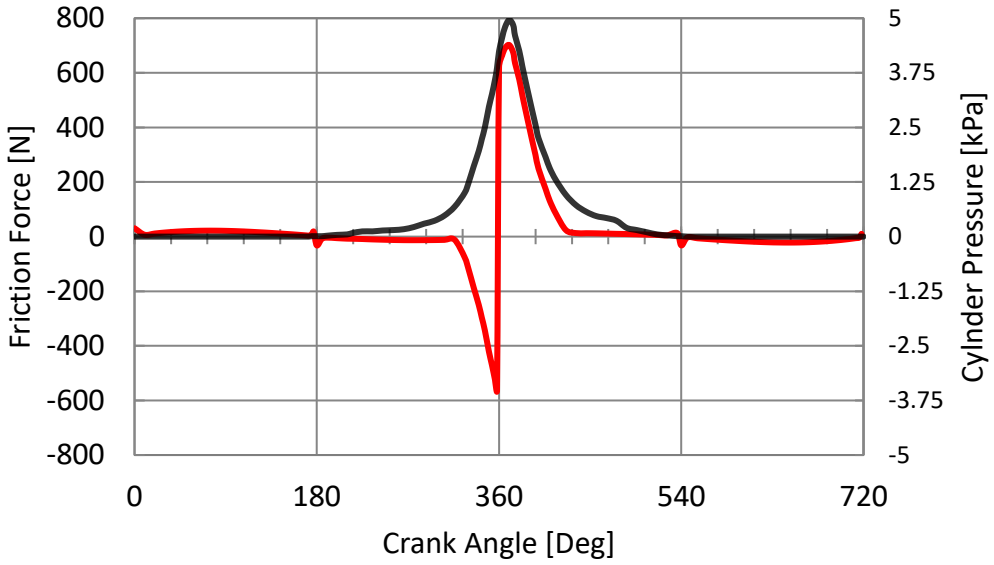

Figure 3.3. Top piston ring friction force (red) and cylinder pressure trace (black).

Figures 3.4 and 3.5 show the friction forces for the second ring and the oil ring. They show comparable values due to the similarity in all parameters except ring tension and ring contact area, in which the oil ring has a higher tension and slightly smaller contact area. The transition from hydrodynamic lubrication to mixed/boundary lubrication is much more prevalent because of the lower pressures the two piston rings exert on the cylinder wall. The most intriguing part of these figures is the near doubling in friction force during hydrodynamic lubrication, which is the result of increased oil shearing as the piston reaches maximum speed at mid-stroke.

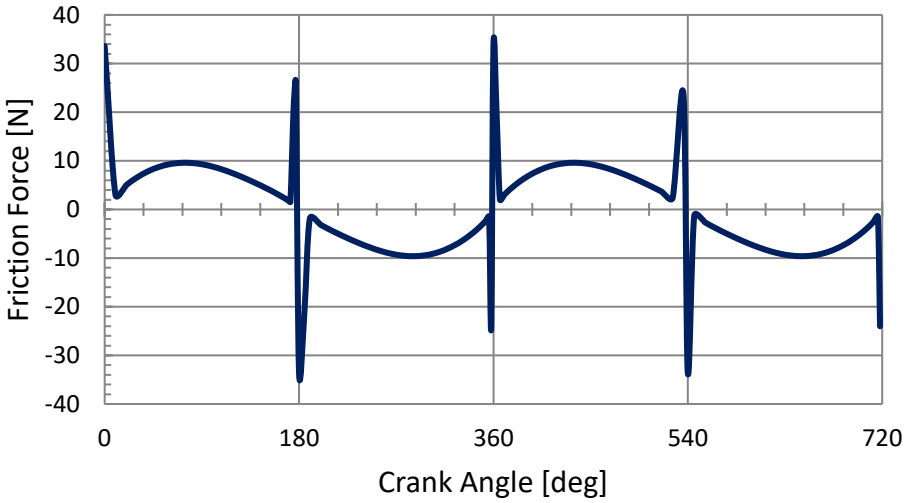

Figure 3.4. Second piston ring friction force per cycle.

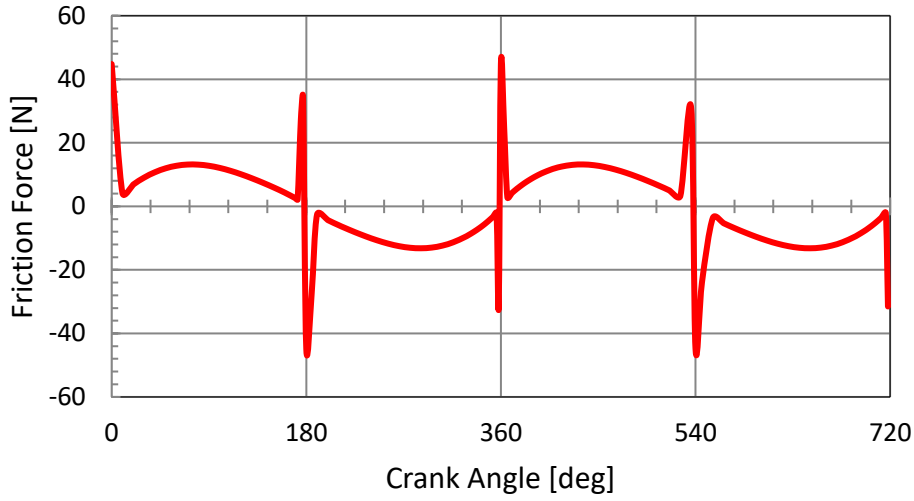

Figure 3.5. Oil ring friction force per cycle.

3.A.2. PISTON SKIRT FRICTION CONTRIBUTION

The piston skirt friction was calculated using Equation 2.22, Equation 2.23, and Figure 2.5. Table 3.2 lists the piston dimensions needed in order to use both equations along with the corresponding values found when using Equation 2.23 and Figure 2.5.

Skirt Max Diameter	0.1018	[m]
Skirt Recess Length	0.0001	[m]
Skirt Shearing Length	0.035	[m]
Scp	3.12E-04	
Fcp	3125	

Table 3.2. Piston skirt dimensions and parameters.

Figure 3.6 shows the calculated piston skirt friction for the engine cycle at 1000 rpm.

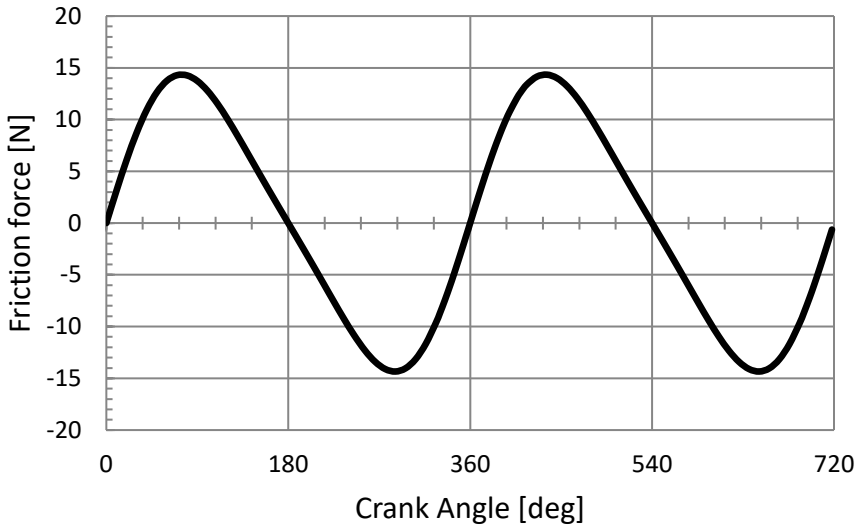

Figure 3.6. Piston skirt friction force per cycle at 1000rpm.

When comparing Figure 3.6 to Figure 2.8 (a piston skirt friction model used in Stanley and colleagues paper), there is considerable difference in friction force values. In Figure 2.8 the engine examined by Stanley and colleagues (1999) is cycling at half the speed used in Figure 3.6 and yet their friction force values are still much higher. Further examination found this is almost entirely caused from selection in oil viscosity. As an example, the parameters used in Figure 3.6 were recalculated, but substituted in the oil viscosity used by Stanley and colleagues (1999) (SAE 30 @ 75º C; μ=0.15 mPa-sec) and it was observed that maximum friction forces begin to exceed 100 N as shown in Figure

3.7. These observations clearly demonstrate the sensitivity of piston skirt friction to oil viscosity and oil selection.

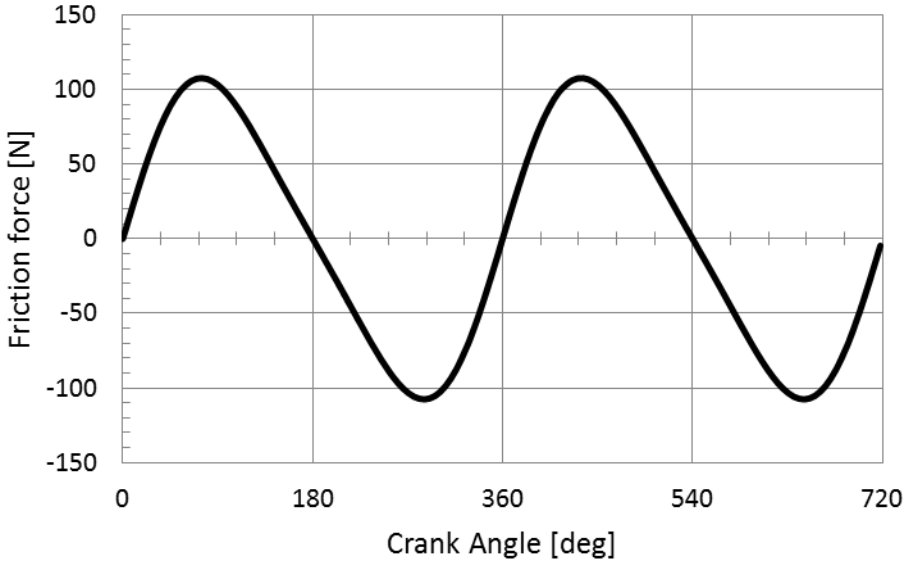

Figure 3.7. Piston skirt friction force at 1000 rpm using μ=0.15 mPa-sec.

3.A.3. LINER JOURNAL BEARING AND FACE SEAL CONTRIBUTION

The RLE uses three journal bearings to allow smooth movement of the rotating liner. The equations for calculating friction forces of journal bearings are readily available in most engineering design text books.

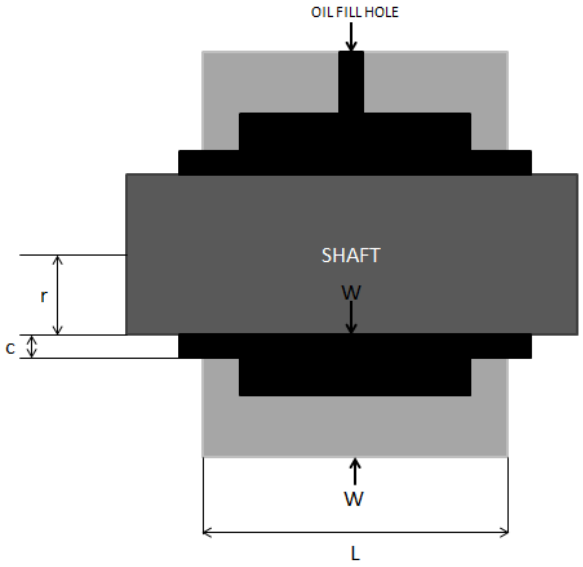

Figure 3.8. Typical journal bearing diagram showing key dimensions.

Using the dimensional variables labeled in Figure 3.8, Equation 3.1 shows how to calculate the torque attributed to journal bearing friction.

$$T = \frac{4\pi^2 r^3 l \mu N}{c} \tag{3.1}$$

Table 3.3 lists the dimensions used in Equation 3.1 to find the friction torque created by the rotating liner journal bearings.

Rotating Liner Journal Bearing Parameters		
c	5.08E-05	[m]
r	0.0542	[m]
L	0.0885	[m]
μ	0.02	[Pa-s]

Table 3.3. Rotating liner journal bearing parameters.

Figure 3.9 shows the friction torque created by the rotating liner journal bearings at varying engine speeds when set to a 3:1 speed reduction relative to engine rpm.

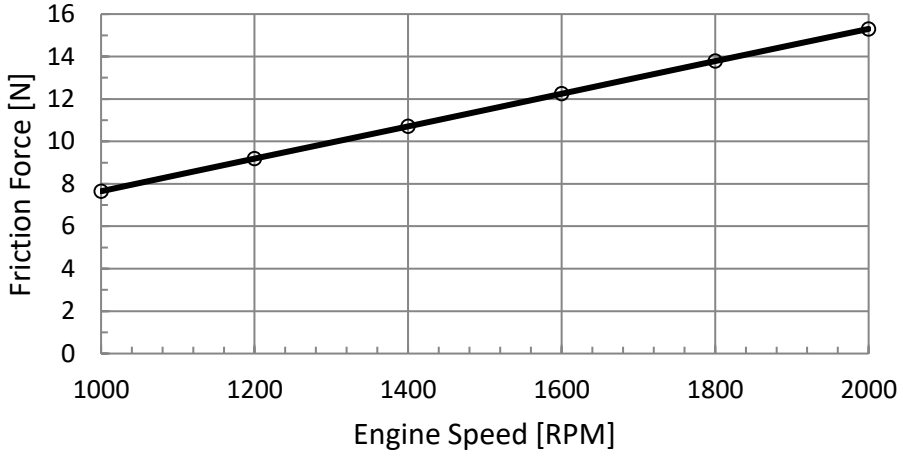

Figure 3.9. Rotating liner journal bearing friction force with liner rotation set to 3:1 reduction from crank speed.

The face seal and liner axial supports have minimal friction torque and are simplified to constant frictional forces. There is a 3.4 N force acting on both surfaces provided by the array of springs nested in the cylinder head; this setup is shown in detail in the appendix. The total frictional torque contribution from the face seal and liner axial support is calculated using Equation 1.7 and multiplying the friction force by the radius of the cylinder. This calculation results in a total frictional torque contribution of 6.6 N-m.

3.A.4. TOTAL PISTON ASSEMBLY FRICTION FORCES AND LINER TORQUE

Summing the piston rings and piston skirt yield Figure 3.10, this is the total estimated piston assembly friction force per cycle of the baseline Cummins 4BT. The trend is similar to the friction force of the top piston ring because of its relatively large magnitude compared to the other factors.

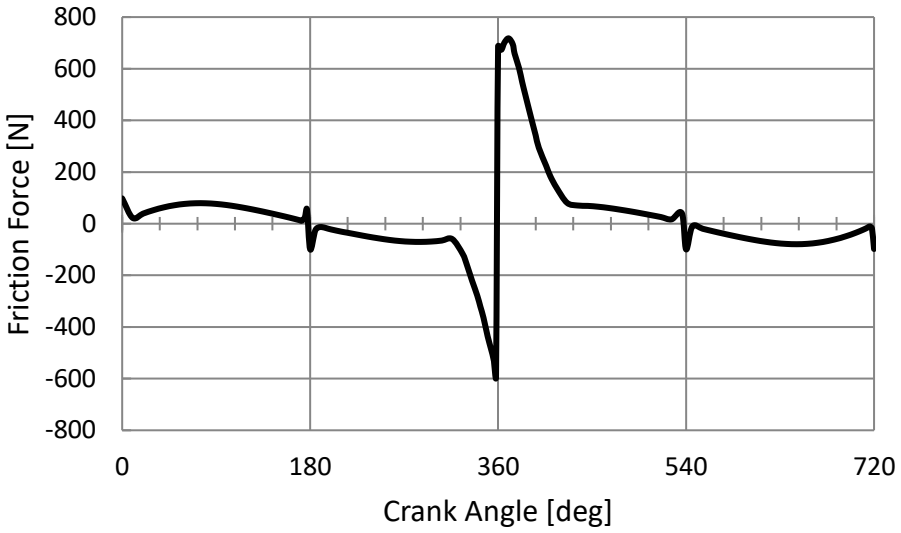

Figure 3.10. Estimated baseline engine total instantaneous piston assembly friction per cycle at 1200 RPM.

The main benefit of the RLE is that it eliminates boundary friction during the piston reversal events. In an attempt to incorporate this characteristic so an estimation in RLE piston assembly friction could be made, the duty parameter was modified to account for the total magnitude of piston speed in the linear and rotational direction. That is, the root sum square of the linear piston velocity and the tangential velocity of the liner was used in place of the piston velocity in calculation of the duty parameter, meaning the piston velocity will be equal to the tangential velocity of the rotating liner at the dead centers. This produced the desired effect of eliminating duty parameter values associated with boundary lubrication and high values for mixed lubrication. Figure 3.11 shows the results of the duty parameter modification on piston assembly friction.

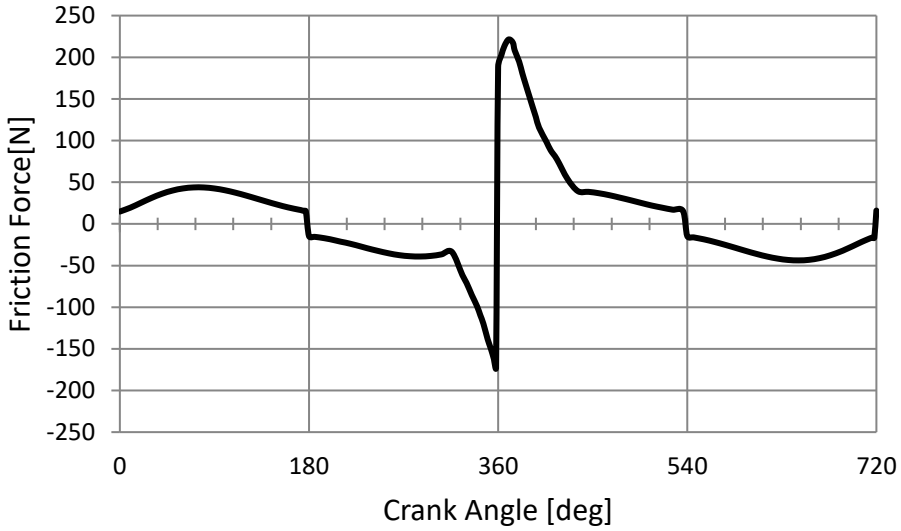

Figure 3.11. Estimated RLE total instantaneous piston assembly friction force per cycle at 1200 RPM

Even with a significantly lower friction coefficient at the piston reversal events, there is still rather large friction force seen around TDC of the compression stroke. Nonetheless, it does decrease the maximum friction force at compression TDC by over seventy percent in comparison to Figure 3.10.

The instantaneous friction force model was varied over several engine speeds to observe its effects. Figure 3.12 shows the average friction forces found from 850 RPM to 2000 RPM. The baseline calculations agree well with the trends seen in Stanley and colleagues (1999) results, validating the calculations have been done in the same manner as stated in their paper. It is useful to note the RLE has a higher reduction in friction force at lower engine speeds; this is an expected result due to the liner rotation reducing the increased amount of mixed lubrication that is associated with lower engines speeds.

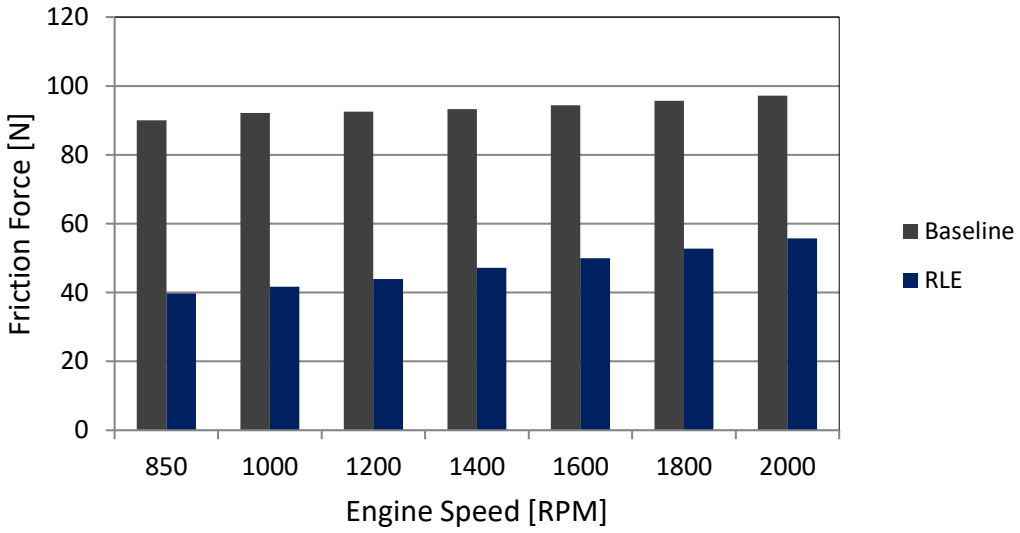

Figure 3.12. Estimated average friction force of piston assembly.

The next planned experimentation of the Cummins 4BT RLE is to measure the torque needed to rotate the cylinder liner. By using the friction force estimates for the RLE shown in Figure 3.12, the friction force can be multiplied by the effective gear radius of the rotating cylinder (0.058 m) to find the estimated parasitic torque of the rotating cylinder liner. Figure 3.13 shows the estimated torque for various engine speeds.

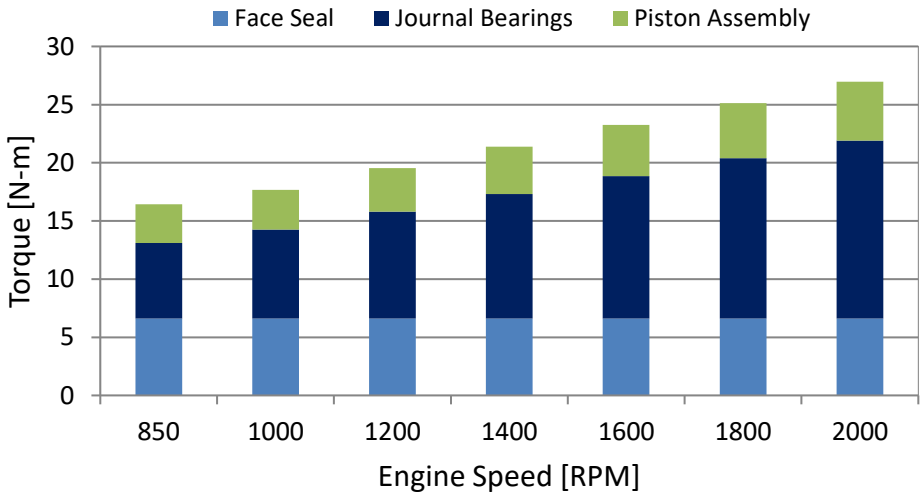

Figure 3.13. Estimated parasitic torque of the rotating liner.

Assuming the piston assembly friction estimates are reasonably accurate, the dominating force contributing to liner torque is the journal bearings. This could prove useful when future RLE liner prototypes are designed since the journal bearing dimensions could be optimized (if not already) for greater reduction in liner drag.

3.B. FMEP Estimation

The fmep model developed by Patton, Nitschke, and Heywood was used to recreate the calculations made during the Quad 4 baseline and RLE experimentation. After validating these results, the fmep model is applied to the Cummins baseline and RLE to predict fmep values as reference for when future experimentation is performed on these engines.

3.B.1. Model Comparison

The Patton, Nitschke, and Heywood model is compared to hot motoring data from the Quad 4 baseline and RLE previously recorded by Kim and colleagues (2005). The constants associated with each friction term were not calibrated for this specific engine and therefore are used as stated in Patton and colleagues' paper. The modified Shayler, Leong, and Murphy model is not compared to the Quad 4 data because the calibrated constants used in their model are for diesel engines with a large degree of different engine parameters. Figure 3.14 shows the Patton, Nitschke, and Heywood model along with the measurements recorded by Kim and colleagues.

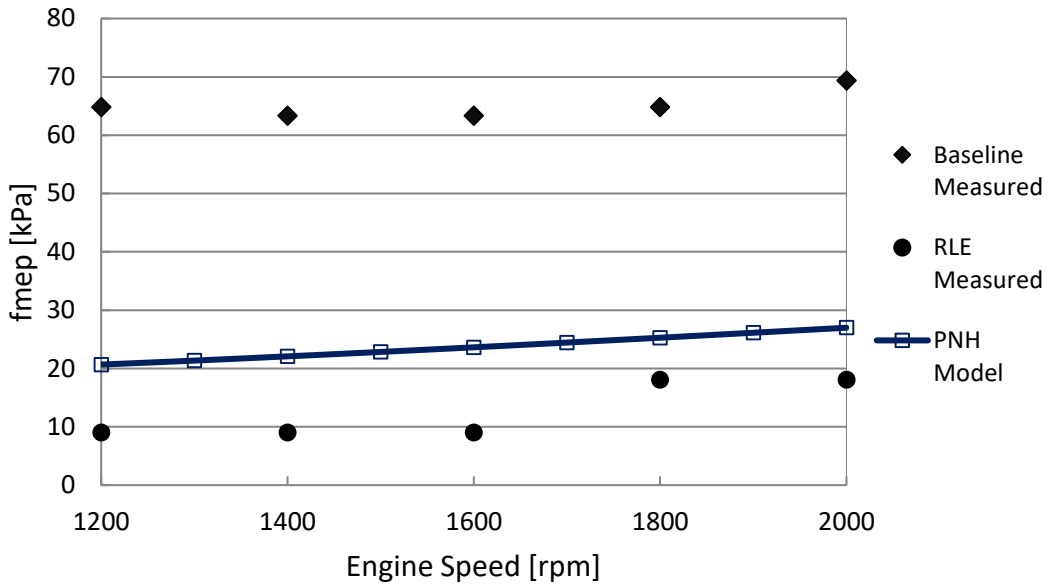

Figure 3.14. Comparison of models to Quad4 baseline and RLE measurements.

As noted by Kim and colleagues (2005), the fmep recorded for the Quad 4 baseline is significantly greater than predicted by the Patton, Nitschke, and Heywood model. Their explanation for measurement and model deviation is stated as possible experimental error, but assure results were repeated with two separate dynamometer setups. Kim and colleagues (2005) also explain the large reduction in friction measurements between the baseline and RLE is not only attributed to elimination of boundary lubrication at the dead centers but also due to larger oil film thickness between the liner and piston skirt at mid-stroke. The larger film thickness reduces oil shearing effects and therefore significantly reduces friction during the mid-stroke portions of the engine cycle.

Assuming the change in reduction in friction between the Quad 4 baseline and RLE is accurate, the percent change can be applied to the Patton, Nitschke, and Heywood model and modified Shayler, Leong, and Murphy model to provide a best-case-scenario estimation in fmep measurements of the Cummins 4BT RLE.

3.B.2. ESTIMATED CUMMINS 4BT BASELINE AND RLE FMEP

The modified model created by Shayler, Leong, and Murphy was used to estimate fmep of the Cummins 4BT baseline and RLE. The modified model created by Shayler, Leong, and Murphy is a better representation of the Cummins 4BT compared to the original Patton, Nitschle, and Heywood model since the calibrated constants associated with each friction term were calibrated using a diesel engine similar to the Cummins 4BT. Figure 3.15 shows the estimated fmep of the baseline and RLE. The Patton, Nitschle, and Heywood model (again using the friction term constants stated in their paper) was also used to estimate fmep of the baseline engine to show the effect that calibrating constants to a specific engine can have on the results.

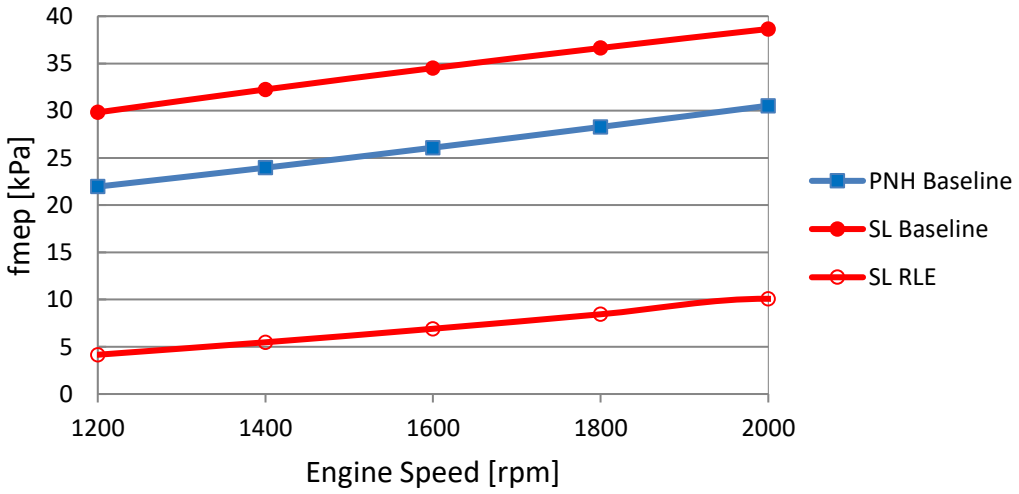

Figure 3.15. Estimated fmep for the Cummins baseline and RLE.

The RLE fmep estimates use the reduction percentages found at each engine speed of the Quad 4 experiment (conducted by Kim and colleagues) in combination with the Shayler, Leong, and Murphy fmep model. The results shown in Figure 3.15 provide a base value of expected fmep for future experimentation of the Cummins 4BT baseline

and RLE. However, it is difficult to say if the reduction in fmep for the RLE will achieve values as low as estimated due to the discrepancies in results discussed in Section 3.B.1.

CHAPTER 4: COMMERCIAL APPLICATION

The ultimate goal for this technology is to see it successfully implemented into a production engine. This chapter examines the various entry routes that could lead it into a commercial market. The benefits have been clearly outlined throughout this report, but with any invention there needs to be a viable market opportunity for it to succeed commercially. This chapter will look at potential markets, those markets' overall interest, and commercialization hurdles the RLE may need to overcome to become a viable commercial option.

4.A. Potential Commercial Markets

4.A.1. Heavy Duty Diesel Engine Manufacturers

The heavy duty diesel engine manufacturing market covers a wide variety of diesel engines. Most companies manufacture diesel engines for multiple applications, such as highway vehicles, power generation, and locomotives. However, each manufacturer covers a group of applications which usually overlaps a portion of another company's group of applications. Top manufacturers in the heavy duty diesel engine industry include Cummins, Caterpillar, Navistar, MAN, and Komatsu. Last year, this industry produced approximately $17.1bn in revenue, and shows only 1.6% in present growth (Peterson, 2016). This low growth corresponds to the maturity of the industry and the saturation of well entrenched businesses within it. The general market concentration for each application is shown below:

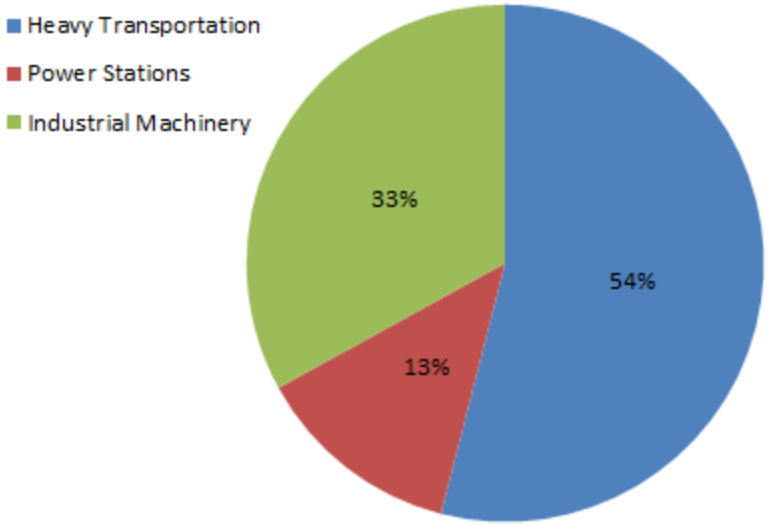

Figure 4.1. Market application for heavy duty diesel engines (Peterson, 2016)

Heavy duty transportation is a very important sector in this industry not only because it is the largest of the three, but also because it is the sector most affected by the increasingly stricter emissions policies. Manufacturers are already working to implement engines compliant with new coming EPA regulations. Furthermore, a rise in fuel prices would increase demand for fuel efficient engines. Reduced emissions and improved fuel efficiency can serve as a growth opportunity for the industry since buyers of diesel engines will invest in methods to save on rising fuel costs. Companies producing products with the more emissions friendly and more efficient engines will be most likely to stay competitive and increase revenues.

4.A.2. Global Ship and Boat Building

The ship and boat building industry has a much smaller focus in diesel engine manufacturing but nonetheless relies heavily on engine performance. Even though some industry leaders outsource to heavy duty diesel engine manufactures specializing in ship engines, these specialized engine manufactures are interlinked with the ship building

industry enough to warrant a separate overview. Industry leaders include Wärtsilä, MAN, Hyundai Heavy Industries, and Mitsubishi Heavy Industries.

Lead time for building a ship usually spans two to three years. This requires manufacturers to be aware of the latest technological advances in shipbuilding, as well as technical and performance characteristics, including technologies to improve fuel economy. The lead time also creates a backlog of orders that extends several years out which gives the industry a uniquely sluggish response to economic conditions (IBISWorld, 2016).

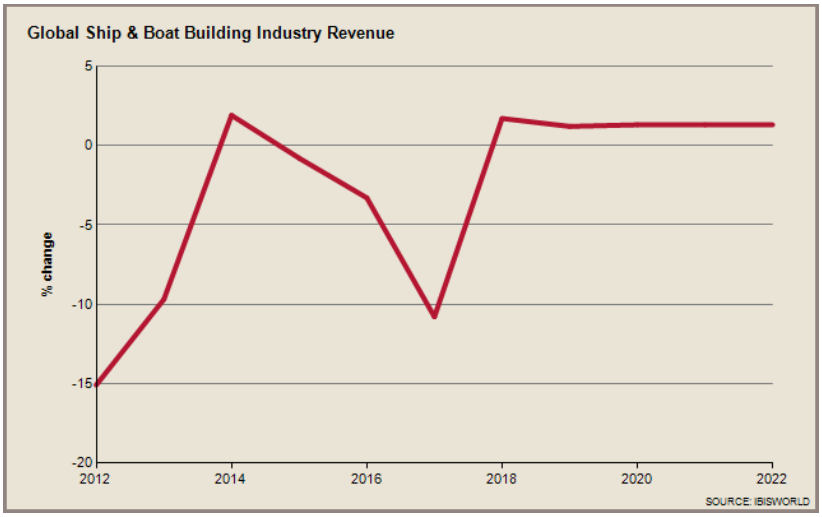

Figure 4.2. Percent change in Global ship and boat building industry revenue (IBISWorld, 2016)

As seen in figure 4.2, it wasn't until 2011 and 2012 that the industry was fully affected by the 2008 global financial crisis and in this current year seeing effects from the slowdown in trade in 2014 and 2015. This correlates directly to the amount of money these companies can invest in R&D opportunities like the RLE.

Although there has been shrinkage in R&D resources in recent years, companies do collaborate with other industrial partners and universities to maximize R&D funds and

develop new technologies (Wärtsilä, 2016). Examples of R&D endeavors for this industry include fuel flexible engines, adaptive power plants, and near-zero emissions engines.

4.B. Market Interest

Over the next five years, IBISWorld expects concentration in the heavy duty diesel industry to grow as the biggest operators in the industry continue to leverage their favorable economies of scale to acquire niche engine developers (Peterson, 2016). This is a favorable outlook for successful testing of the heavy duty diesel RLE since the technology itself is not enough to warrant a full scale company startup operation. Since the industry is broad and many companies manufacture diesel engines for a variety of applications, looking at individual companies with ideal scaling capabilities seems to be the wisest approach to research market interest.

All companies within this industry are on the lookout for technologies to improve engine efficiency. However, due to the uniqueness of the heavy duty diesel RLE solution and the current minimal amount of empirical data to support theoretical improvements, cost of R&D vs. potential benefit will be the primary manner to commercialize the technology. Companies most likely to be interested in this technology will be those that emphasize research and development as a core value along with openness to innovation. Two such manufacturers are MAN and Komatsu.

MAN possesses the ideal diversified line of engines to apply the RLE technology. Their engines span automotive, trucking, and ship building applications. MAN also has a strong focus on research and development to create new products with increased customer value. MAN invested 5% of its revenue to R&D in 2014, which amounted to almost $1bn. Moreover, R&D expenditures continue to rise by more than 10% each year

along with continually increasing employment in this sector of their business (MarketLine, 2016).

Komatsu, although not as diversified as MAN, is another company that exemplifies R&D endeavors. The company is actively involved in research for new technologies, new products and new services consistent with its commitment to provide quality products. Furthermore, Komatsu has also made advances in research relating to energy conservation, component recycling and reuse, and the evaluation of environmental loads through lifecycle assessment techniques (MarketLine, 2016). In particular, Komatsu has placed special emphasis on activities relating to technologies that reduce fuel consumption, which is in direct alignment with the RLE technology.

4.C. Competing Technologies

There are numerous approaches to creating a more fuel efficient and emissions friendly engine. Methods for reducing frictional losses are for the most part cheaper than other efficiency increasing avenues. Two popular and current methods for reducing friction are lowering oil viscosity and thermally sprayed protective cylinder coatings. As discussed earlier in this report, lowering oil viscosity relates to less resistance between rotating and reciprocating parts. Cylinder coatings attempt to lower piston assembly friction by enhancing the cylinder surface finish with more desirable surface finish characteristics. However, the RLE technology is the only one of the three to address solving the underlying friction problem inherent to reciprocating piston assemblies rather than mitigate it.

4.C.1. Lowering Oil Viscosity

Lowering oil viscosity is by far the cheapest method to research and implement when looking to increase engine efficiency. History, models, and results all prove its

effectiveness, but the margins of increased efficiency are not as profound as they once were. The effects of lowering oil viscosity are explained in Chapter 1, where it is also mentioned that the underlying return on investment is on the decline. Currently companies continue to pursue new ways to work around the challenges which increase up-front cost of implementation.

4.C.2. THERMALLY SPRAYED PROTECTIVE CYLINDER COATINGS

Thermally sprayed protective coatings are a relatively modern technology in the automotive industry. Coating the cylinder wall with certain specialized materials increases wear resistance and improves surface finish to reduce piston friction. There are a variety of coating materials that can be applied depending on the application. As an example, heavy duty diesel engines can be coated with a metal matrix composite (MMC) which can be polished to similar standards of cast iron, but have increased porosity to better retain oil along the cylinder wall (Ernst and Fletcher, 2016). Although upfront costs of machinery and materials are higher than implementing lower viscosity oils, it is likely cheaper than adjusting the design of the engine which is the case of the RLE.

4.D. Barriers to Market Entry

The heavy-duty diesel manufacturing industry is in the mature stage of its life cycle and has incredibly high entry barriers for any new manufacturer wanting to join. RLE technology by itself does not warrant such a drastic attempt. As with most technologies created by third party members that improve one aspect of a much larger assembly, and where it is the focus of a single, well entrenched industry, it is safer and more profitable to sell the technology to an industry leader.

The largest hurdle for RLE technology is testing validation. Compared to other proven avenues of technological research in friction reduction, such as oil viscosity, there

has been little cylinder rotation experimentation performed since the early half of the twentieth century done on the sleeve valve engine. The absence of literature to draw upon to support cylinder rotation research makes it a riskier investment than other options. Research on, and demand for the technology will increase significantly if a fully operational prototype is created and multiple tests validate the theoretical estimates in improved efficiency

CHAPTER 5: CONCLUSIONS AND RECOMMENDATIONS

The fundamentals of piston engines are briefly overviewed and history on the rotating sleeve valve engines is given. Specifics of piston assembly friction are discussed and highlight the necessity for lowering piston assembly friction. It is also pointed out that lowering oil viscosity has been a proven method for lower piston assembly friction in the past, but may soon be reaching its beneficial limitations and other methods need to be pursued. Another more innovative approach for reducing piston friction is the Rotating Liner.

The Rotating Liner Engine was designed by Dr. Dardalis as a solution for lowering piston assembly friction. Experiments on a gasoline prototype RLE were performed in 2005 and a new heavy duty diesel prototype will soon be tested in the same manner. This report discusses a couple well known piston assembly friction models and applies them to the gasoline and diesel baseline engines. Estimates based on the gasoline prototype RLE and the models described in this report are given to predict the torque attributed to the rotating liner and piston assembly fmep.

The piston assembly friction models discussed and used in this report are listed below:

1) Piston Assembly FMEP Models developed by Patton, Nitschke, and Heywood (1989)
2) Modified versions of the Piston Assembly FMEP Models by Sandoval and Heywood (2003)
3) Modified versions of the Piston Assembly FMEP Models by Shayler and Leong FMEP Model (2005)

4) Instantaneous Piston Assembly Friction Models developed by Stanley, Taraza, Henein, and Bryzik.

The instantaneous piston assembly friction models were applied to the Cummins 4BT parameters to find total average friction force of the piston assembly. The calculations decently matched trends for values calculated by Stanley and colleagues (1999) for their diesel engine setup; verifying the Cummins 4BT calculations had been performed correctly. An attempt to apply the same models to the prototype RLE was conceived by modifying the duty parameter to account for cylinder wall rotation. This successfully removed high friction coefficient values associated with boundary and mixed lubrication. It did not account for any improved squeeze film phenomena or possible reduced oil film shearing between the piston skirt and cylinder wall that the RLE may induce. The RLE piston friction forces were then summed with the additional components causing friction on the rotating assembly to estimate the torque needed to rotate the liner. It was noted the liner journal bearings contribute the most to liner drag. It would be beneficial to conduct a separate experiment to measure the friction contributions of the journal bearings, face seal, and axial support individually so the amount of piston assembly friction could be found by subtracting these components from the overall torque measurements during normal operating conditions.

The fmep models developed by Patton and colleagues (1989) were first compared to the data recorded by Kim and colleagues (2003). The same conclusions as found by Kim and colleagues (2003) were replicated which confirmed calculations were performed correctly even though the data measurements from the baseline Quad 4 were much higher than predicted by the models. Reasons for the discrepancies were reiterated as stated by Kim and colleagues (2003). The fmep models previously mentioned and also the fmep models presented by Shayler and Leong were applied to the Cummins 4BT baseline

engine. Coupling these estimates with the percent change in fmep found in the Quad 4 experiments yielded fmep estimates for the Cummins 4BT RLE. It was noted these estimates are likely to be slightly lower than what would be measured. When the next round of experimentation occurs for the Cummins 4BT baseline and RLE, the process of adjusting the constants in the Patton, Nitschke, and Heywood model should be performed to better match the model trends to the data measured.

Since the RLE prototype is in its later stages of development, it seemed relevant to discuss the commercial opportunities this technology possesses in this report. Potential markets were listed and then were narrowed down to recommend a few specific companies that may hold a higher interest in adopting the RLE technology. Competing technologies and barriers to market entry were also discussed to highlight possible hurdles that may stop the RLE from being successfully commercialized. Overall, The RLE presents itself as a strong candidate as a next generation engine design once a fully operational prototype can be offered to validate model predictions to present to interested buyers.

APPENDIX A: FUTURE CUMMINS 4BT PROTOTYPE RLE EXPERIMENTAL SETUP

A.A. Future Experimentation

The Cummins 4BT heavy duty diesel RLE prototype has undergone cylinder modifications to alleviate rotating liner seizure problems due to liner expansion from heat of the initial few hundred combustion cycles. Now that the RLE is operational again, an experimental setup will be installed to measure the torque of the rotating liner. This appendix describes the RLE setup along with the future instrumentation that will be used to collect data.

A.A.1. Heavy Duty Diesel RLE Prototype

The heavy duty diesel RLE prototype is constructed similarly to the gasoline RLE. A four cylinder diesel engine is converted to single cylinder operation and modified to use the rotating liner. Bob weights are used to replace the piston assemblies in the three unused cylinders. The four cylinder diesel engine chosen for modification is a 1989 Cummins 4BT. Stock parameters of the engine are listed in Table A.1, below.

Type	Inline 4 cylinder
Displacement (L)	3.9
Stroke (mm)	120
Bore (mm)	102
Compression ratio	17.6:1

Table A.1. Cummins 4BT engine parameters.

Cylinder two in the engine is modified to accommodate the rotating cylinder liner while keeping the same piston size. Figure A.1 shows the top half the rotating liner, two notable features are the rotating liner sealing area with evenly distributed oil groves and

the driven gear directly below the top face. The oil grooves help maintain a film of oil between the rotating liner and the face sealing ring, shown in Figure A.2.

Figure A.1. Rotating liner partially inserted into engine block.

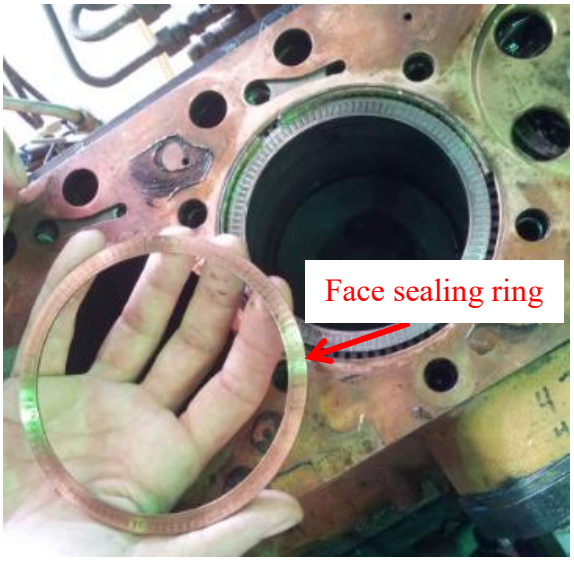

Figure A.2 Face sealing ring being inspected after engine disassembly.

The face sealing ring applies a nominal force onto the rotating liner by a series of springs recessed into the cylinder head. The cylinder head has also been modified to partially insert into the rotating liner in order to prevent combustion gas leakage. Figure A.3 shows proof the head insert correctly sealed in combustion gasses after a previous test run since there is a distinct line where the carbon stopped depositing on the head.

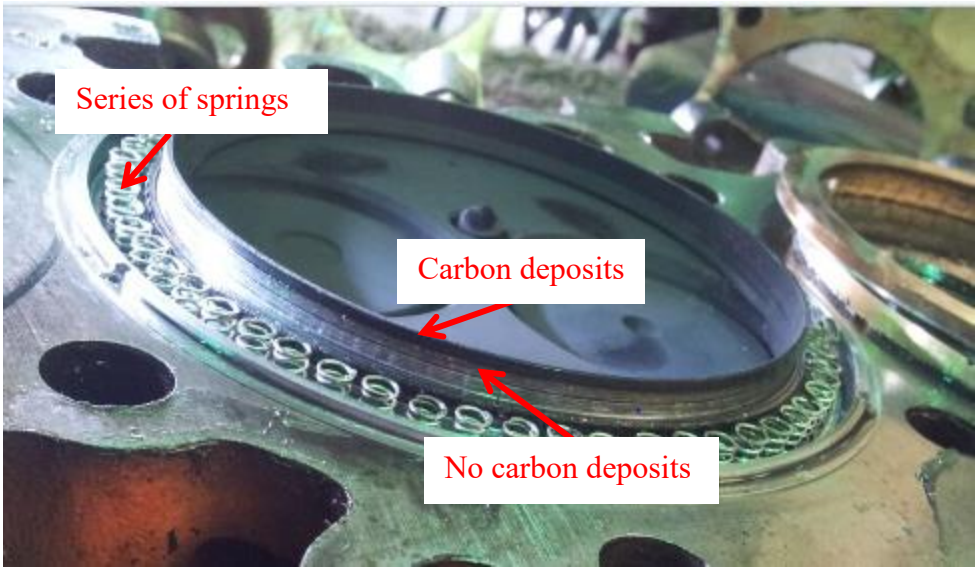

Figure A.3. Head insert and recessed springs.

The drive mechanism is inserted into cylinder one and is driven by an accessory belt as shown in Figure A.4. The gear box transfers the rotation 90 degrees from the accessory belt in order to drive the gear in cylinder one. The gear box also has a reduction ratio of 2:1.

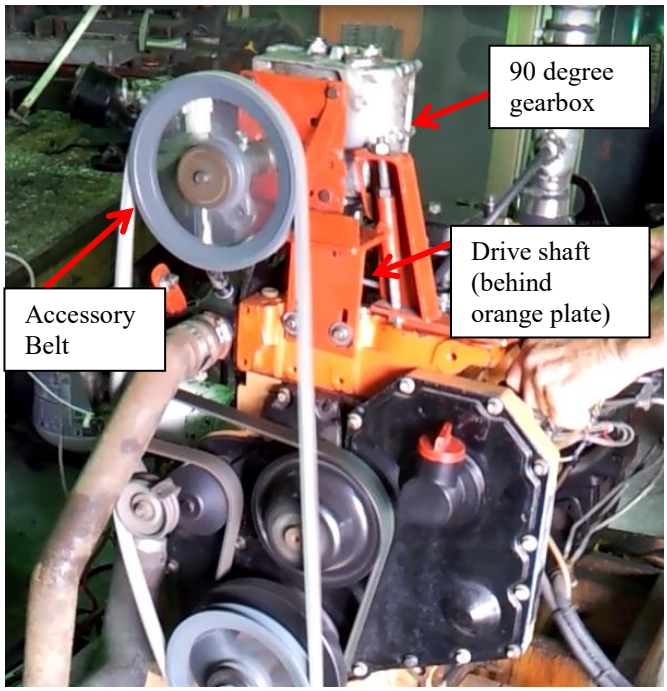

Figure 2.4. Rotating liner drive mechanism.

The Cummins 4BT has a mechanically operated fuel system, limiting adjustments in fuel timing and injected amount. Three injectors were set with varying injection pressures for testing in order to have some variability in injection timing. The injection pressures are 135kPa, 145kPa and 164kPa.

A.A.2. INSTRUMENTATION

In this future series of tests, there are three measurements of interest; cylinder pressure, RPM, and torque from the rotating cylinder liner. The instrumentation setup is shown in Figure A.5.

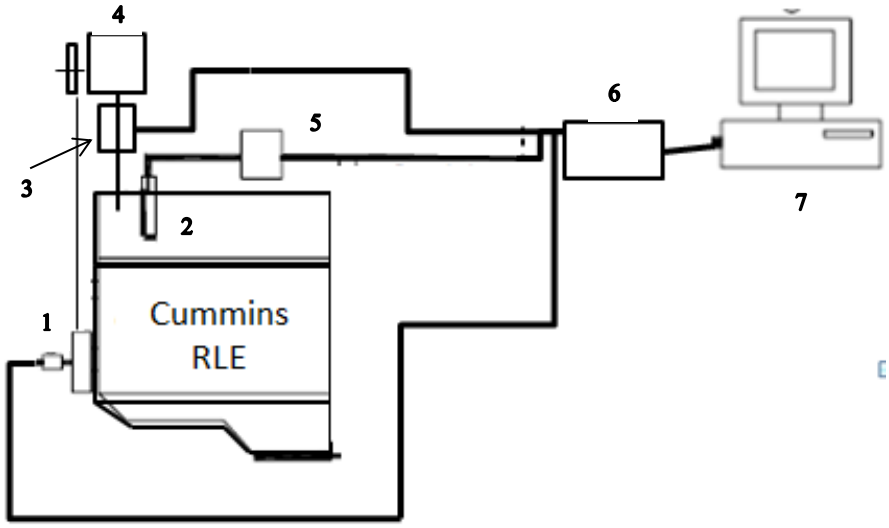

1) Encoder
2) Pressure transducer
3) Torque cell
4) 90 degree gearbox
5) Charge amplifier
6) NI Compact DAQ
7) Personal computer

Figure A.5. Instrumentation setup of RLE testing

An optical encoder is attached to the crank pulley to measure crank RPM. The optical encoder chosen is a BEI H25. A Kistler 6051 pressure transducer is mounted in the cylinder head to measure cylinder pressure. The pressure transducer voltage signal is amplified by a Kistler Type 5051 charge amplifier. A Cooper LTX963 rotating torque sensor will be coupled between the gear box and rotating liner driving mechanism to measure friction torque of the rotating liner. Table A.2 below lists the specifications for the torque sensor. A polymer shaft coupler will couple the torque sensor to the driving mechanism. This will help minimize misalignment issues that can alter torque measurements and also prevent over torqueing the sensor by breaking if exceeding the rated torque limit.

Model	Cooper LXT963
Capacity	2000 in-lbs
Linearity	±0.1% F.S.
Hysteresis	±0.1% F.S.
Repeatbility	±0.1% F.S.
Output	4.1418 mV/V

Table A.2. Torque sensor specifications.

All instruments will send signals to a National Instruments Compact DAQ which interfaces with a personal computer to record and analyze data. Table A.3 lists the NI modules chosen for the Compact DAQ along with the input signals it received.

Model	Description	Input Signal
NI cDAQ-9178	NI CompactDAQ 8-Slot USB Chassis	N/A
NI 9215	±10 V, Simultaneous Analog Input, 100 kS/s, 4 Ch Module	Torque Sensor
NI 9411	±5 to 24 V, Differential Digital Input, 6 Ch Module	Charge amplifier (pressure transducer)
NI 9219	Universal Analog Input, 24-Bit, 100 S/s/ch, 4 Ch Module	Optical encoder

Table A.3. List of NI modules used in Compact DAQ.

REFERENCES

[1] Adams, S.R. "The Centenary Patent- Single-Sleeve Valve Engines." World Patent Information (2010)

[2] Bishop, I., "Effect of Design Variables on Friction and Economy," SAE Technical Paper 640807, 1964, doi:10.4271/640807.

[3] Burke, C., Nagler, L., Campbell, E., Lundstrom, L. et al., "WHERE DOES ALL THE POWER GO?," SAE Technical Paper 570058, 1957, doi:10.4271/570058.

[4] Caterpillar Company Profile. (2016, August 19). Retrieved October 06, 2016, from Marketline.

[5] Cleveland, A. and Bishop, I., "SEVERAL POSSIBLE PATHS TO IMPROVED PART-LOAD ECONOMY OF SPARK-IGNITION ENGINES," SAE Technical Paper 600355, 1960, doi:10.4271/600355

[6] Cummins Company Profile. (2016, August 19). Retrieved October 6, 2016, from Marketline.

[7] Dardalis, D., Matthews, R., and Lebeck, A., "Design Details of the Compression Ignition Rotating Liner Engine. Reducing Piston Assembly Friction and Ring/Liner Wear in Heavy-Duty Diesel Engines," SAE Technical Paper 2012-01-1963, 2012, doi:10.4271/2012-01-1963.

[8] Dardalis, D., Matthews, R., Kiehne, T., and Kim, M., "Improving Heavy-Duty Engine Efficiency and Durability: The Rotating Liner Engine," SAE Technical Paper 2005-01-1653, 2005, doi:10.4271/2005-01-1653.

[9] Global Ship & Boat Building. (2016, April). Retrieved October 06, 2016, from IBISWorld.

[10] Iris, P. "Cruise Control: The Industry Will Record Steady Growth as Volatile Revenue Swings Settle down." Heavy-Duty Diesel Engine Manufacturing in the US (2016): n. pag. IBISWorld. Web. 06 Oct. 2016.

[11] Jeng, Y., "Friction and Lubrication Analysis of a Piston- Ring Pack," SAE Technical Paper 920492, 1992, doi:10.4271/920492.

[12] Kim, M., Dardalis, D., Matthews, R., and Kiehne, T., "Engine Friction Reduction Through Liner Rotation," SAE Technical Paper 2005-01-1652, 2005, doi:10.4271/2005-01-1652.

[13] Komatsu Company Profile. (2016, September 30). Retrieved October 06, 2016, from Marketline.

[14] Malagi, R., Kurbet, S., and Krishnakumar, R., "A Comprehensive Model to Study the Dynamic Motion of Piston and Friction and Lubrication in I.C.Enignes," SAE Technical Paper 2008-28-0061, 2008, doi:10.4271/2008-28-0061.

[15] MAN Company Profile. (2015, December 18). Retrieved October 06, 2016, from Marketline.

[16] Marek, S., Henein, N., and Bryzik, W., "Effect of Load and Other Parameters on Instantaneous Friction Torque in Reciprocating Engines," SAE Technical Paper 910752, 1991, doi:10.4271/910752.

[17] Marshall, E.L., (2013) A Lifelong Love Affair — Sir Harry Ricardo and the

[18] Sleeve Valve, The International Journal for the History of Engineering & Technology, 83:1, 62-95, DOI: 10.1179/1758120612Z.00000000020.

[19] McGeehan, J., "A Literature Review of the Effects of Piston and Ring Friction and Lubricating Oil Viscosity on Fuel Economy," SAE Technical Paper 780673, 1978, doi:10.4271/780673.

[20] Meloni, M., Cacciatore, D., Dohmen, J., Ring, F. et al., "Lamborghini Approach to Engine Downsizing Engine Friction Modeling," SAE Technical Paper 2013-24-0088, 2013, doi:10.4271/2013-24-0088.

[21] Patton, K., Nitschke, R., and Heywood, J., "Development and Evaluation of a Friction Model for Spark-Ignition Engines," SAE Technical Paper 890836, 1989, doi:10.4271/890836.

[22] Payri, F., Lopez, J., Pla, B., and Graciano Bustamante, D., "Assessing the Limits of Downsizing in Diesel Engines," SAE Technical Paper 2014-32-0128, 2014, doi:10.4271/2014-32-0128.

[23] Permude, A., Pathak, M., Kumar, V., and Singh, S., "Influence of Low Viscosity Lubricating Oils on Fuel Economy and Durability of Passenger Car Diesel Engine," SAE Int. J. Fuels Lubr. 5(3):1426-1435, 2012, doi:10.4271/2012-28-0010.

[24] Rakopoulos, C., Hountalas, D., Koutroubousis, A., and Zannis, T., "Application and Evaluation of a Detailed Friction Model on a DI Diesel Engine with Extremely High Peak Combustion Pressures," SAE Technical Paper 2002-01-0068, 2002, doi:10.4271/2002-01-0068.

[25] Sandoval, D. and Heywood, J., "An Improved Friction Model for Spark-Ignition Engines," SAE Technical Paper 2003-01-0725, 2003, doi:10.4271/2003-01-0725.

[26] Shayler, P., Leong, D., and Murphy, M., "Contributions to Engine Friction During Cold, Low Speed Running and the Dependence on Oil Viscosity," SAE Technical Paper 2005-01-1654, 2005, doi:10.4271/2005-01-1654.

[27] Stanley, R., Taraza, D., Henein, N., and Bryzik, W., "A Simplified Friction Model of the Piston Ring Assembly," SAE Technical Paper 1999-01-0974, 1999, doi:10.4271/1999-01-0974.

[28] Stanton, D., "Systematic Development of Highly Efficient and Clean Engines to Meet Future Commercial Vehicle Greenhouse Gas Regulations," SAE Int. J. Engines 6(3):1395-1480, 2013, doi:10.4271/2013-01-2421.

[29] Tamminen, J., Sandström, C., and Nurmi, H., "Influence of the Piston Inter-ring Pressure on the Ring Pack Behaviour in a Medium Speed Diesel Engine," SAE Technical Paper 2005-01-3847, 2005, doi:10.4271/2005-01-3847.

[30] Taraza, D., Henein, N., and Bryzik, W., "Friction Losses in Multi-Cylinder Diesel Engines," SAE Technical Paper 2000-01-0921, 2000, doi:10.4271/2000-01-0921.

[31] Tian, T., Rabute, R., Wong, V., and Heywood, J., "Effects of Piston-Ring Dynamics on Ring/Groove Wear and Oil Consumption in a Diesel Engine," SAE Technical Paper 970835, 1997, doi:10.4271/970835.

[32] Ting, L.L. (1993), "Development of a reciprocating test rig for tribological studies of piston engine moving components - Part 1: rig design and piston ring friction coefficients measuring method", SAE Paper 930685; also in: Tribology of Engines and Engine Oils, SAE Special Publication SP-959.

[33] Xu, H., Kim, M., Dardalis, D., Bryant, M., Matthews, R., & Kiehne, T. (2005, April 5). Numerical and Experimental Investigation of Piston Ring Friction. ASME 2005 Internal Combustion Engine Division Spring Technical Conference. doi:10.1115/ICES2005-1086